AECL-10215

ATOMIC ENERGY OF CANADA LIMITED

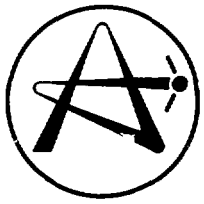

ÉNERGIE ATOMIQUE DU CANADA LIMITÉE

A MODIFIED GAUSSIAN MODEL FOR THE THERMAL PLUME FROM A GROUND-BASED HEAT SOURCE IN A CROSS-WIND

MODÈLE GAUSSIEN MODIFIÉ DESTINÉ À L'ÉTUDE DU PANACHE THERMIQUE ÉMANANT D'UNE SOURCE DE CHALEUR AU SOL DANS UN VENT LATÉRAL

W.N. SELANDER, P.J. BARRY and E. ROBERTSON

Chalk River Nuclear Laboratories

Laboratoires nucléaires de Chalk River

Chalk River, Ontario K0J 1J0

June 1990 juin

ATOMIC ENERGY OF CANADA LIMITED

A MODIFIED GAUSSIAN MODEL FOR THE THERMAL PLUME FROM A GROUND-BASED HEAT SOURCE IN A CROSS-WIND

by

W.N. Selander, P.J. Barry* and E. Robertson*

*Environmental Research Branch
Waste Management Systems
Chalk River Nuclear Laboratories
Chalk River, Ontario, Canada K0J 1J0

1990 June

AECL-10215

ÉNERGIE ATOMIQUE DU CANADA LIMITÉE

MODÈLE GAUSSIEN MODIFIÉ DESTINÉ À L'ÉTUDE DU PANACHE THERMIQUE ÉMANANT D'UNE SOURCE DE CHALEUR AU SOL DANS UN VENT LATÉRAL

par

W.N. Selander, P.J. Barry* et E. Robertson*

RÉSUMÉ

Un réseau de brûleurs au gaz propane fonctionnant au sol, dans un vent latéral, a été utilisé comme source de chaleur pour obtenir un panache thermique soumis à l'action du vent. Un réseau tridimensionnel de thermocouples a permis d'assurer la mesure en continu de la température du panache sous le vent par rapport à la source. On s'est servi des résultats obtenus pour effectuer la corrélation des paramètres du modèle gaussien modifié relatifs à l'ascension et la dispersion d'un panache avec les paramètres d'intensité de la source, de la vitesse du vent et de la dispersion atmosphérique.

*Recherche sur l'environnement
Systèmes de gestion des déchets
Laboratoires nucléaires de Chalk River
Chalk River (Ontario) Canada K0J 1J0

Juin 1990

EACL-10215

ATOMIC ENERGY OF CANADA LIMITED

A MODIFIED GAUSSIAN MODEL FOR THE THERMAL PLUME FROM A GROUND-BASED HEAT SOURCE IN A CROSS-WIND

by

W.N. Selander, P.J. Barry* and E. Robertson*

ABSTRACT

An array of propane burners operating at ground level in a cross-wind was used as a heat source to establish a blown-over thermal plume. A three-dimensional array of thermocouples was used to continuously measure the plume temperature downwind from the source. The resulting data was used to correlate the parameters of a modified Gaussian model for plume rise and dispersion with source strength, wind speed, and atmospheric dispersion parameters.

*Environmental Research Branch
Waste Management Systems
Chalk River Nuclear Laboratories
Chalk River, Ontario, Canada K0J 1J0

1990 June

AECL-10215

TABLE OF CONTENTS

LIST OF TABLES

LIST OF FIGURES

1. INTRODUCTION

This report describes a set of experiments and their interpretation, involving the thermal plume generated by an array of propane burners operating at ground level. The experiments were done in strong winds, so the plume did not rise directly but was blown over. A three-dimensional array of thermocouples was placed downwind of the burners to continuously measure plume temperatures.

The original incentive for the work was the need to predict the performance of the Gas Dispersion Systems (GDS) located at AECL's heavy-water plants, which the burner system was designed to simulate in small scale. Early investigations revealed a lack of understanding of plumes from a ground-based, spatially distributed source in a cross-wind, and there were, therefore, a number of scientific questions to be answered. Following the decommissioning of the heavy-water plants, direct interest in GDS performance ended; however, the scientific questions remained, with potential applications elsewhere. Their investigation forms the basis of this report.

An array of burners located on or near the ground and operating in a cross-wind generates a buoyant plume, whose behaviour can be to some extent analysed in the same way as the plume from an elevated stack or chimney. These have been studied extensively [see Briggs (1969), Beychok (1979), Turner (1970)]. The burner plume is, however, more complex because it originates from a distributed source rather than a point, and is initially ground-based. These two factors, which are necessary for a GDS to function effectively by surrounding and trapping a possible contaminant release, modify the lift and entrainment processes considerably. In this report, the important plume parameters are identified and correlated with the data, leading to a model of plume behaviour that can be extrapolated to systems of larger scale.

The experimental arrangements are described in Section 2 of the report, and the treatment of the data is described in Section 3. The general approach to modelling the plume is outlined in Section 4, and the correlations of various plume parameters with the data are given in Sections 5, 6, 7 and 8. Appendix A contains details of the propane burner system. Appendix B contains details of the mathematical treatment of plumes that are nearly Gaussian in distribution. Appendix C contains a list of symbols used in the mathematical model and a summary of the equations obtained.

2. EXPERIMENTAL

The experimental data were obtained using a three-dimensional array of thermocouples. These were mounted 50 cm apart on poles set into the ground at 10° intervals, on arcs of circles at varying distances from the centre (Figures 1a and 1b). The data-logger (an extended Campbell Scientific CR7) could accept up to 445 thermocouple inputs. This limited the size and density of the thermocouple array that could be used. Several designs were tried to optimize the area covered consistent with an adequate density of sensors within the area. The final design and the one used for most of the trials consisted of six arcs at distances of 2.5, 5.0, 7.5, 10.0 and 15.0 m. The 2.5 m arc was abandoned when the diameter of the burner ring exceeded 2.0 m.

The innermost arc consisted of 5 poles, giving an angular coverage of 40°. Seven thermocouples were mounted on each pole, to a height of 3.0 m. Each of the other arcs contained nine poles, giving an angular coverage of 80°. The centre pole of every arc was mounted so as to be downwind of the most frequent wind direction, roughly NW. Each pole on the 5.0 and 7.5 m arcs had eight thermocouples to 3.5 m, while each of those on the 10.0 and 12.5 m arcs had nine thermocouples to 4.0 m. Eleven thermocouples on each pole of the 15.0 m arc gave a vertical height to 5.5 m. Each thermocouple was fitted with a simple radiation shield (Figure 2).

For the first three experiments, an arc at 25.0 m was instrumented, but at this distance, the measured plume temperatures were difficult to distinguish from those of the ambient air, and 15.0 m was selected as the furthermost measuring distance from the centre.

Also in the early experiments, two sets of poles were set up to give coverage for both NW and SE winds. Because of the limited number of thermocouples that the data-logger could accept, it was then only possible to have five poles on each set of arcs and those could only be instrumented to 2.5 m. Because the mean wind did not always flow along the centre of the arcs, and because of the large turbulent fluctuations of horizontal wind direction, the centre of the thermal plume in the horizontal plane could not always be clearly identified. Furthermore, the height of rise of the heated plume was often such that the centre of the plume in the vertical plane could likewise not be identified.

Accordingly, the set of arcs NW of the centre was removed and the thermocouples thus released were used to expand the SE arcs laterally and vertically, as earlier described. This change meant that experiments could only be run during NW winds, but the increased proportion of useful trials more than offset this one disadvantage of the new layout.

Each thermocouple was electric arc-welded at one end of a copper-constantin thermocouple wire. The other end of the wire was fed through the hollow centre of the pole to reach ground level, where it terminated at a standard copper-constantin connector. Bundles of thermocouple wire cable connected the thermocouple to the data-logger inputs through another connector block just before the wires entered the data-logger housing. Altogether, over 10 miles of thermocouple wire were used.

The data-logger itself was kept in a small trailer about 25 m west of the thermocouple array. Air conditioning in summer and heating during spring and fall kept the data-logger at a more or less constant temperature during the experiments.

In most experiments, between 25 and 50 thermocouple assemblies malfunctioned. Two major causes of malfunctioning were identified. The screws holding the thermocouple wires on the data-logger input terminal block loosened, causing a poor connection. A possible cause of this was the wide fluctuations of temperature in the trailer during the often long intervals between runs when the air conditioning was off. The other major cause of malfunctioning was breaks in thermocouple wires.

Most often this occurred near a connector and could be repaired, but sometimes the break occurred along the cable and could not always be repaired.

The data-logger scanned the thermocouple array in less than 0.01 s. It contained an internal reference junction, the absolute temperature of which was obtained using a built-in thermistor. Using an internal program, the data-logger calculated the absolute temperature at each thermocouple and wrote it onto an audio magnetic tape in a standard audio cassette recorder. Although each scan was very rapid, the time taken to do the calculations and prepare an output meant that scans could only be repeated at roughly 35 s intervals. At the end of a day's experiments, the magnetic tape was played back through an interface, to send the information to the CRNL main-frame computer, a CDC CYBER 175, for filing and further examination.

3. TREATMENT OF WIND AND TEMPERATURE DATA

3.1 Presentation of Data

During the test series, various wind conditions and source configurations were chosen, and the temperature profiles were collected continuously over long periods, typically one-half hour, for each set of conditions. For convenience in later analysis, these wind and temperature profiles were divided into (nominal) ten-minute means. Approximately 100 individual tests were obtained in this way, of which the majority ($\simeq$70) corresponded to circle or point sources. These "standardized" tests and their parameters are listed in Tables 1 and 2.

3.2 1983 Wind Data

Anemometers were located at 0.43 m, 0.64 m, 1.43 m and 3.00 m above ground. Wind speeds were given as five-minute averages, which were weighted and mixed to give ten-minute averages coinciding with the ten-minute temperature means. Visual inspection of the data showed the wind profiles to be closely logarithmic, with, however, some bending near the top. Although there is a plausible physical explanation for this, it may also be due to instrument error, since the anemometer at 3.00 m occasionally gave readings that were obviously too low. Therefore, all profiles were assumed to be of the standard logarithmic form (Pasquill (1974)).

$$U(z) = (U_*/k) \ln (z/z_o), \quad k \simeq 0.4 \qquad (3.1)$$

Preliminary plots showed the roughness lengths z_o for the various profiles to be closely clustered. For each group of tests, therefore, a mean value of z_o was assumed and the friction velocity U_* for each test was determined graphically. The value of z_o varied from 1.3 cm (south winds) to 2.0 cm (north winds). The terrain at the CRNL sites consisted of a mixture of short grass, longer grass and bare earth, and the above values are consistent with those reported in the literature for similar conditions.

3.3 1984 Wind Data

The anemometers were recalibrated between the 1983 and 1984 seasons, and their number increased to six, located at 0.65, 1.32, 1.90, 2.58, 3.15 and 3.83 m above ground. The individual wind data represented one-minute samples, which were averaged to form ten-minute means coinciding with the temperature means. The standard deviation of each ten-minute mean was generally between 15 and 25% of the mean. The ten-minute profiles were well-represented by a logarithmic curve, with some evidence of bending near the top, indicating decreased shear due to atmospheric instability. The mean roughness length was taken as 1.0 cm for all tests.

In summary, therefore, the wind profiles were closely logarithmic, with roughness lengths of the value expected for the terrain, 1.0 to 2.0 cm. The relative standard deviation of the ten-minute means was roughly 20%. Typical logarithmic wind plots for the two years are shown in Figures 3 and 4.

3.4 Corrections to Ten-Minute Temperature Means

To ensure a reasonably clean set of data for the fitting and modelling process, the time-consuming and labour-intensive task of scrutinizing the data and eliminating serious errors was undertaken. Apart from scatter caused by normal instrument variation and environmental fluctuations, two types of error were recognized:

(i) readings that were clearly incorrect or spurious, usually caused by sudden failure of thermocouples or other instruments, and

(ii) readings that were suspect because of consistent unexplained differences, which usually indicated the early stages of thermocouple failure. During the tests, it was realized that an increasing number of thermocouples were failing, particularly in the line nearest the burners. In many cases, these failures were not obvious at first, and could only be detected by a gradual drift occurring over a sequence of tests.

The above errors were eliminated by interpolation among adjacent sites. Finally, the mean corrected temperatures were reduced to local temperature differences by subtracting the mean ambient temperature.

A large number of temperature profiles (too many to report individually) were generated, as described above. A sampling of the output is provided in Figures 5a to 5g.

Tables 1 and 2 include all tests with the burners placed in circles and lines. It was found, however, that most of the line sources were, in fact, at an angle to the intended cross-wind direction and therefore did not satisfy the assumptions of symmetry. For this reason, the analysis in the following sections of the report is based on the data from the circle and point sources only.

4. PLUME DEVELOPMENT AND MODEL

4.1 Plume Development

Each burner produces a plume that emerges into a cross-wind as a pre-mixed flame. The flame or jet trajectory depends initially on its momentum, but the effects of buoyancy and entrainment soon dominate its behaviour. Depending on burner spacing, the individual burner plumes eventually merge into a collective plume whose behaviour is of primary interest for the interpretation of data and for GDS performance. In Section 7 of Appendix A, it is shown that, for the burners used in this study, the initial rise due to jet momentum is approximately,

$$\Delta z_J = L_m \tag{4.1}$$

where

$$L_m = 0.89 D_J U_J / U(0.3) \tag{4.2}$$

is the momentum length scale. Combustion has a small effect on the initial trajectory, and is neglected in deriving Eq. (4.1).

In the following stage, the merged plume rises and spreads in a way that is limited by source geometry and by contact with the ground. This near-field stage can be visualized from the results of Rankine (1950) and Rouse (1947), who measured temperatures downwind from a line of burners placed across the floor of a wind tunnel. They found the near field to be essentially two-dimensional, with the temperature plume in contact with the ground, where the maximum temperatures occurred. The plume depth was found to be proportional to the downwind distance x, with a proportionality constant that depended on the densimetric Froude number for the source; see Thomas (1964). In the present notation, the Froude number is,

$$F = [g\epsilon NQ/L\rho c_p T_a U^3]^{-\frac{1}{4}} \tag{4.3}$$

These early experiments did not provide any data on the transition from the initial ground-based two-dimensional stage to the elevated (i.e., detached) three-dimensional stage. The small-scale water flume experiments by Slawson (1986), and references cited therein, show that lift-off is initiated by enhanced entrainment as the plume deepens. Depending on the source geometry, the plume sides may then begin to roll up, driven by horizontal temperature gradients, and form two counter-rotating vortices. This further enhances entrainment from the sides and diminishes the relative importance of the part of the plume still in contact with the ground; complete lift-off quickly follows. During this period, the centreline of the plume undergoes transition from a linear dependence on x to a 2/3 power law, which is characteristic of buoyant rise.

Once the plume detaches from the ground and becomes roughly circular in cross-section, it rises and entrains the surrounding air in a very similar way to the plume from an elevated stack. The literature on such plumes is extensive, the main result being that the centreline trajectory is determined by the scaling law,

$$z_c = AL_B^{1/3}x^{2/3} \tag{4.4}$$

where

$$L_B = [g\epsilon NQ/\rho c_p T_a U^3] = L/F^2 \tag{4.5}$$

is the buoyancy length characteristic of the source in an ambient wind of speed U. The coefficient A will, however, depend on the initial source distribution, or equivalently on the source Froude number. Slawson (1986) correlated the results for ring and line source configurations and found that the lift-off distance, x_L, is given by

$$x_L \simeq 1.1LF \tag{4.6}$$

4.2 Plume Model

The present study aims to derive a plume model that correlates the data in a physically meaningful way, and can be extrapolated to systems of a significantly larger scale. Plume analysis has taken one of two basic approaches. One approach, originated by Morton et al. (1956), is a deterministic model, based on differential equations for the evolution of mass, momentum and energy in a plume element. This model identifies important plume parameters such as buoyancy length and ambient Froude number, and requires a "plume entrainment constant", which can be determined from the data. The model was used in the early analysis of the GDS plume, by DSMA (1975) and Selander (1978). The details of the model have been given by Slawson (1976, 1986) and others.

An alternative approach that has been successful in describing the atmospherically-induced dispersion of plumes from elevated point sources is the Gaussian or statistical model (see, e.g., Turner (1970), Beychok (1979)). The concentration at a distance x downwind from a continuous point source located at the origin of Cartesian coordinates is proportional to:

$$[2\pi U\sigma_y\sigma_z]^{-1}\exp[-\tfrac{1}{2}(y/\sigma_y)^2]\left[\exp[-\tfrac{1}{2}(z-z_c)^2/\sigma_z^2]+\exp[-\tfrac{1}{2}(z+z_c)^2/\sigma_z^2]\right] \tag{4.7}$$

where the "plume rise" $z_c(x)$ has been given by various formulas (see Beychok (1979), Briggs (1969)). The x-dependence of the horizontal and vertical atmospheric dispersion parameters σ_y and σ_z is given in the reference cited, for various weather categories. Eq. (4.7) has the advantage of a standardized form that automatically conserves heat or mass.

Preliminary analysis showed that atmospheric mixing had considerable effect on the plume observed in this work, and this posed a problem for the interpretation of the "entrainment constant" required for the deterministic model. Therefore, the plume was modelled by Eq. (4.7) using, however, modified dispersion parameters Σ_y and Σ_z in place of σ_y and σ_z. The modified parameters were correlated with source (buoyancy) parameters, and with the atmospheric dispersion parameters σ_y and σ_z. The numerical correlation of these quantities, and of the plume centreline $z_c(x)$, is described in the following sections.

5. ANALYSIS OF CROSS-WIND (LATERAL) TEMPERATURE DISTRIBUTIONS

According to the model described in the previous section, the profiles of the lateral or cross-wind variation of the temperature rise above ambient can be expressed in the following form,

$$\Delta T(x,y,z) = f(x,z)\ \exp[-\tfrac{1}{2}(y/\Sigma_y)^2] \qquad (5.1)$$

where Σ_y is a modified Gaussian parameter that combines the effect of initial source width and subsequent dispersion. The function $f(x,z)$ is considered in a later section. In Appendix B, it is shown that Σ_y depends on the source dimension L and the "point-source" dispersion parameter σ_y, through the formula,

$$\Sigma_y = \sigma_y[1 + a(L/\sigma_y)^2] \qquad (5.2)$$

where "a" is a coefficient depending on source configuration. For a ring source of diameter L, a = 1/16.

Analysis of the data shows the observed values of Σ_y are independent of z, and the values of σ_y obtained by solving (5.2) depend on the downwind distance x in a manner characteristic of atmospheric dispersion, and are uncorrelated with source parameters. In other words, the lateral or cross-wind dispersion from the sources is essentially atmospheric, and independent of elevation.

These conclusions were obtained by dividing the mean temperatures taken from the three-dimensional downwind grid into sets of two-dimensional profiles taken at the fixed distances x = 2.5 m, 5.0 m, 7.5 m, 10.0 m, 12.5 m, 15.0 m and 25.0 m. Due to limitations of equipment, not all tests were done at all of these distances. Since the temperature sensors conformed to polar coordinates, the two-dimensional profile at each downwind distance was measured on a (θ,z) grid. For each value of z, the temperature rise above ambient was fitted on a horizontal "line-by-line" basis, using a simple Gaussian function, with $\Sigma_y = x\Sigma_\theta$ as described in Appendix B, that is, with Eq. (5.1) written as,

$$\Delta T(\theta) = A\ \exp[-\tfrac{1}{2}(\theta-\theta_o)^2/\Sigma_\theta^2] \qquad (5.3)$$

The cross-wind dispersion coefficient, obtained by solving Eq. (5.2),

$$\sigma_y(x) = \tfrac{1}{2}[x\Sigma_\theta + (x^2\Sigma_\theta^2 - L^2/4)^{\frac{1}{2}}] \qquad (5.4)$$

was then evaluated at each distance for each test.

Only point and circle sources (69 cases in all) were analyzed in this way, since the line sources were sufficiently askew to the mean wind direction to invalidate the above simple assumptions, particularly Eq. (5.2).

The following observations were made:

(i) The least squares fits (using the CRNL subroutine NL2INT) were generally successful, and gave anomalous fits or failed to converge in relatively few cases. This usually happened where the signal was weak, e.g., at large distances from the source or far away from the plume centreline, or where a few spurious data points remained.

(ii) There was no overall correlation of σ_y with source dimension L or source strength NQ.

(iii) The angular dispersion parameters Σ_θ are essentially independent of z, except near z=0 where the effect of using a mean ambient temperature to convert measured temperature into temperature rise has the effect of increasing Σ_θ on warm days and decreasing it on cold days. This is explained by the fact that on warm days (when most of the tests were done) the ground and the air nearest to it were warmer than ambient; consequently, the temperature differences obtained by subtracting a fixed background were larger near the ground, causing the plume to appear broader. The reverse happened on cold days when frost or residual cold remained in the ground as the air temperature increased; this was observed less frequently. As expected, there was an overall sensitivity to small errors in ambient temperature. Rejecting these obviously biased points, and a few others affected by spurious data, the value of Σ_θ for each value of x used in Eq. (5.4) was obtained by averaging of the line-by-line fitted values over z.

The values of σ_y for each series of tests and each distance x are given in Tables 3 to 8, with the mean values and standard deviations for each distance. Table 9 gives the overall weighted mean values of σ_y in metres, at each distance x, and the overall standard deviation in metres.

The mean values σ_y are plotted in Figure 6. For comparison, graphs of atmospheric dispersion parameters σ_y, taken and extrapolated from standard references, are also drawn. At these small distances, σ_y is proportional to $x^{0.9}$, approximately. The Pasquill-Gifford curve for class A weather, based on 3-minute averages, gives σ_y(100.0 m) = 27.0 m. The IAEA Safety Guide gives σ_y (100.0 m) = 24.0 m, based on one-hour averages in class B weather. The formula that relates the atmospheric dispersion parameter σ_y to the standard deviation σ_θ about the mean wind direction is

$$\sigma_y = 0.045\ \sigma_\theta(x^{0.86})$$

where x is given in metres. Comparing this formula with the (weighted) overall mean for the tests suggests that $\sigma_\theta \simeq 11.5°$ for all distances, which is in the range (10° - 15°) considered to represent neutral conditions.

Although it would require separate, and site-specific, measurements to confirm it, all of the above evidence (especially the resemblance to the Pasquill-Gifford curve and lack of correlation with NQ or L) points to the conclusion that the lateral plume spread in these tests is governed by atmospheric dispersion, rather than buoyancy, and that atmospheric conditions for the tests were generally neutral or unstable.

6. ANALYSIS OF PLUME CENTRELINES

6.1 The Data

The peaks of the lateral Gaussian fits to the 10-minute temperature means, previously described, gave a vertical distribution whose maximum, according to usual practice, was defined as the plume centreline trajectory $z_c(x)$. The location of the maximum was determined by a combination of visual and numerical interpolation, at each downwind distance x = 2.5 m, 5.0 m, etc. In this section, $z_c(x)$ is analysed and correlated with the appropriate variables. Included in the analysis are data from all circular sources, including "point" sources as limiting cases.

6.2 Reference Wind Velocity

It was initially expected that the effect of the wind shear associated with the logarithmic velocity distribution could be included in the analysis of z_c in a meaningful way. Preliminary analysis using a "local" wind speed $U(z_c)$ to characterize the plume variables did not, however, appear to yield any useful information that could not be obtained using a reference velocity at a fixed height. Therefore, the results are presented using the velocity U_2 determined at z = 2.0 m as a reference. The failure of a continuously varying U(z) to improve the analysis is probably due to scatter in the results.

6.3 Burner Height and Jet Momentum Corrections

The observed trajectories $z_c(x)$ were corrected for the burner height, 0.20 m. In addition, as discussed in Section A.7 of Appendix A, and in Section 4.1, the plume trajectory in a cross-wind is initially a jet dominated by the exit momentum of the burner and, to a lesser degree, by buoyancy. In practically all cases considered, the transition between initial jet behaviour and buoyant plume behaviour was fairly abrupt and the momentum effect could also be eliminated by subtracting a correction from $z_c(x)$. This correction was found to depend mainly on burner output, and was chosen as 0.20 m at a nominal burner power of 0.132 MW and 0.25 m at a nominal burner power of 0.173 MW. This choice represents a compromise and may account for some of the scatter in the final centreline correlation. The corresponding horizontal correction is negligible on the scale of distance involved.

6.4 Buoyancy Parameters

For a fully merged plume, the corrected centreline $z'_c(x)$, equal to the observed $z'_c(x)$ minus the above corrections, depends only on buoyancy and should, therefore, be completely characterized by the buoyancy length,

$$L_B = \epsilon NgQ/\rho c_p T_a U^3 \quad (6.1)$$

and the source diameter L, or alternatively by the densimetric Froude number, which from Eq. (4.3) and (4.5) can be written,

$$F = (L/L_B)^4 \quad (6.2)$$

For the "point" sources, in which the experiment was performed with the burners piled together as closely as possible, an effective source diameter L≃0.5 m was assigned, so that a meaningful Froude number could be defined.

It is expected that $z'_c(x)$ would satisfy a correlation of the form

$$z'_c/L_B = f(x/L_B, F) \quad (6.3)$$

Before determining the "best" form of the function $f(x/L_B, F)$, the dimensionless distances z'_c/L_B and x/L_B were examined for possible residual correlations with other variables such as burner spacing, wind speed and burner power. No significant correlations were found, although some of the near-field scatter appeared to be related to burner spacing and jet momentum. Combustion and variations of wind direction appear to cause sufficiently rapid mixing to obscure any systematic effects beyond the first row of temperature sensors.

6.5 Correlation of $z'_c(x)$

The form chosen for $f(x/L_B,F)$ will depend on further information in the form of a plume-rise model. For a small elevated source, e.g., a stack, the well-established model is (see Briggs (1969))

$$z'_c/L_B = A(x/L_B)^{2/3}, \ A = \text{constant} \quad (6.4)$$

The plumes in this study originate near ground level from a source of finite diameter, and both of these effects must be accounted for. As noted in Section 4.1, the proximity to the ground will cause the plume to initially form a quasi-2D regime where z'_c is proportional to x, with the ratio (z'_c/x) depending on F. The dilution and subsequent modifications in plume rise caused by the source size will be reflected in the dependence of A on F in (6.4), which represents the asymptotic plume rise.

Accordingly, the plume is assumed to pass through an initial line source or "2D" stage, followed by a transitional stage where lift-off occurs, or at least where the ground ceases to affect the plume significantly, and finally into a "fully elevated" stage where the usually 2/3 law is expected to govern. From the work of Slawson (1986), the lift-off distance is approximately

$$x_L \simeq 0.8\ LF \qquad (6.5)$$

During the initial period (before x_L), the plume rises like a wedge and the centreline has a form that is in reasonable agreement with early wind-tunnel results (Rankine (1950), Rouse (1947), Thomas (1964)). The near-field points in the data gave the following equation:

$$z'_c = 0.27xF^{-\frac{1}{3}} \qquad (6.6)$$

Of course, the transition to the elevated plume is not abrupt and is influencing the plume even in the "2D" stage. Therefore, for purposes of matching with a transitional stage, it is expected that the effective length of the initial stage will be shorter than indicated by (6.5), and from the data it appears that the transition length,

$$x_T = 0.6\ LF \qquad (6.7)$$

is a good choice. The general shape of the plume is sketched in Figure 7.

The initial stage centreline $z'_c(x)$ is therefore given by (6.6), for $x<x_T$ as given by (6.7). The transition height z_T is given by:

$$z_T = z'_c(x_T) = 0.27\ x_T F^{-\frac{1}{3}} = 0.16\ LF^{\frac{1}{3}} \qquad (6.8)$$

Beyond the transition point (x_T, z_T) at which the plume may be considered essentially free of ground effects, it will undergo further evolution to the asymptotic 2/3-law (6.4). The asymptotic form suggested by earlier tests analysed by Selander (1977) is

$$z'_c/L_B \simeq (C/F^{1/3})(x/L_B)^{2/3} \qquad (6.9)$$

where C is a constant. Accordingly, the variables chosen beyond the transition point were $(x-x_T)/L_B/F$ and $(z'_c-z_T)/L_B$. Figure 8 shows all the observations plotted in this manner, for all point sources L=0.5 m, 1.0 m, 2.0 m, 3.0 m and 4.0 m. The correlation is free of any bias or skewness related to L. The dozen or so points that fail to cluster around the main curve, especially at the lower end, in all cases occur near the transition point, indicating some lack of consistency in the choice of transition. This is understandable since the plume rise in the 2D regime is linear, whereas the correlation in Figure 8 indicates a more rapid dependence for small $(x-x_T)/L_B/F$. The near-field points would be the most susceptible to error in any transition model. Notwithstanding the above limitations, the correlation appears to give a reasonably consistent description of the observed centrelines.

6.6 Correlation Equation

The curve shown in Figure 8, with the ±25% error bars, is given by the formula

$$Z = 0.9\ X^{2/3}/[1 + 3.0/X^{2/3}] \qquad (6.10)$$

where

$$X = (x-x_T)/L_B F^{\frac{1}{4}}, \quad Z = (z'_c - z_T)/L_B \tag{6.11}$$

This suggests that the distance required for the ground-free plume to evolve to its asymptotic height, as well as the asymptotic behaviour, is scaled to $X^{2/3}$. The coefficient 0.9 for the asymptotic rise is larger than observed for the results reported by Selander (1977), however, the difference can be explained by the choice of reference velocities.

6.7 Alternative Correlations

The correlations represented by (6.10) is not the only possible interpretation of the centreline data. An initial plot of z'_c/L_B vs x/L_B gave exponents larger than 2/3, which were uncharacteristic of buoyant rise, and contained factors that were not dimensionless with respect to L even when allowances were made for proximity to the source. This clearly showed the need for a more careful analysis of the near field. A further attempt was made to correlate terms of the form $(z'_c/L_B)F^n$ vs $(x/L_B)F^m$, and the best reduction to the data to a single curve was achieved with n=1/2, m=0. This implies, however, that the distance required for transition to the asymptotic 2/3 law is independent of L, which is unrealistic. The overall correlation (not shown graphically) can be fitted by a function of the form,

$$z'_c/L_B = 0.95(x/L_B)^{2/3}F^{-\frac{1}{4}} \tanh [0.25 \sqrt{(x/L_B)}] \tag{6.12}$$

The asymptotic constant 0.95 is close to the one obtained in (6.10), which shows that the asymptotic far-field prediction is the same for both models.

6.8 Discussion

A correlation has been found, based on a reasonable physical model, which contains most of the centreline data within error margins of $\pm$25%. It exhibits no residual correlations with any test variables other than L_B and F, and exhibits a high degree of cohesion between experiments with different source diameters. The scatter in the correlation is attributed to normal experimental error, unmeasured environmental factors, and errors in fitting, smoothing and interpolation, as well as possible errors in assigning corrections for initial jet behaviour of the individual burner flames. Some of the scatter, especially in the near field, is due to simplifications made in the model that describes the transition from the initial "2D" regime. Notwithstanding the above scatter, the correlation and its equation appear to describe the centreline trajectory as a function of L_B and L in a consistent and physically meaningful way, and is recommended for extrapolation of the scale model results.

7. ANALYSIS OF VERTICAL TEMPERATURE PROFILES

7.1 The Model

The Gaussian model for downwind temperature distribution, as described in Section 4, with modified dispersion parameters Σ_y and Σ_z, is

$$\Delta T(x,y,z) = \frac{[\epsilon NQ/\rho c_p]}{2\pi U \Sigma_y \Sigma_z} \exp[-\tfrac{1}{2}(y/\Sigma_y)^2]\{\exp[-\tfrac{1}{2}(z-z_c)^2/\Sigma_z^2]+\exp[-\tfrac{1}{2}(z+z_c)^2/\Sigma_z^2]\} \quad (7.1)$$

As described in the previous two sections, the data has been used to correlate the cross-wind parameter $\Sigma_y(x)$ and centreline height $z_c(x)$ with the appropriate source and environmental parameters. In this section, the dependence of the modified vertical dispersion parameter Σ_z will be identified and correlated. In the analysis, the velocity U in (7.1) will be chosen as the wind speed U_c at the local centreline height $z_c(x)$. This choice is made because the centreline corresponds to the maximum temperature, and because the wind speed varies relatively slowly with height, at least for the elevated part of the plume.

The second Gaussian in (7.1) is the "ground reflection" term, resulting from the assumption that the plume transfers no heat to the ground. This term is generally unimportant for $z>z_c$.

The maximum downwind vertical temperature profile is obtained by setting y=0 in (7.1),

$$\Delta T_o(x,z) = \frac{[\epsilon NQ/\rho c_p]}{2\pi U_c \Sigma_y \Sigma_z} \{\exp[-\tfrac{1}{2}(z-z_c)^2/\Sigma_z^2]+\exp[-\tfrac{1}{2}(z+z_c)^2/\Sigma_z^2]\} \quad (7.2)$$

The observed profiles ΔT_o computed from the data, as described in Section 5, were of the general shape predicted by (7.2). They were characterized by a small residual temperature near the ground (measured at z=0.1), rising to a fairly well-defined peak identified as the plume centreline, with a decrease at higher levels. There was some skewness about the peak, especially in the near field.

7.2 Energy Conservation

The overall heat balance at each downwind distance x is given by

$$U_c \rho c_p \iint_{yz} \Delta T(x,y,z)dydz = \epsilon NQ \quad (7.3)$$

To check that the data satisfies this for the expected value $\epsilon = 0.88$, it is sufficient to integrate over the observed vertical profiles $\Delta T_o(x,z)$ since the validity of the Gaussian distribution in y has already been confirmed in Section 5. Integration of (7.2) gives

$$\int_0^\infty \Delta T_o(x,z)dz = (2\pi)^{-\frac{1}{2}}[\epsilon NQ/\rho c_p \Sigma_y U_c] \tag{7.4}$$

All factors on the right side of (7.4) have been previously determined, with an allowance for temperature dependence of the air density ρ. The accuracy of the integration of ΔT_o in (7.4) was limited by scatter in the data, and because the thermocouple array missed an estimate 10 to 20% of the upper tail of the plume. A simple approximate trapezoidal rule was therefore devised for the integration, and applied to a random sample of about 10% of the measured profiles. It shows that (7.4) was confirmed to within $\pm$20%, with a few exceptions in the very near field, caused by incipient thermocouple failure, as already noted. The mean value of the balance confirmed a burner efficiency factor between 0.85 and 0.90. Although there is some evidence of vertical skewness in the ΔT_o profiles, suggesting that Σ_z may vary with z, the scatter in the heat balance was too large to permit useful quantitative estimates of it to be made.

7.3 Identification and Correlation of Σ_z

The value of Σ_z is most easily defined at the maximum (smoothed) temperature rise $\Delta T_o(x,z_c) = \Delta T_{max}(x)$. From (7.2), then,

$$\Sigma_z(x) = \frac{[\epsilon NQ/\rho c_p]}{2\pi\Sigma_y(x)U_c\Delta T_{max}(x)}\{1+\exp[-2(z_c/\Sigma_z)^2]\} \tag{7.5}$$

If $z_c/\Sigma_c \geq 1.3$, approximately, the image term can be neglected, so that

$$\Sigma_z(x) = \epsilon NQ/\rho c_p 2\pi\Sigma_y(x)U_c\Delta T_{max}(x) \tag{7.6}$$

In the majority of profiles, with exceptions in the near field, (7.6) was used to compute Σ_z from the data.

The values of Σ_z obtained from (7.6) or (7.5) were used to check the profiles above and below the centreline. As noted earlier, there was some skewness towards higher values of z; however, this may reflect some loss of heat to the ground, or it may be related to the shear in the wind profile.

The dependence of Σ_z on plume parameters L_B and L (or F), as well as on downwind distance x, was examined. For most of the data, the centreline equations can very roughly be expressed as

$$z_c \simeq 0.2x \tag{7.7}$$

which shows that the source subtends a relatively small vertical angle when viewed from a point on the downwind centreline. Accordingly, Σ_z was not expected to depend strongly on the source dimension L, and was correlated with x and L_B in the form,

$$\Sigma_z / L_B = f(x/L_B) \tag{7.8}$$

The reference value of L_B, based on the 2 m wind speed, was used in (7.8). As will be seen, the correlation is nearly linear, so that a refinement such as using a local wind speed is unnecessary. This was verified by a subsequent check. The lack of correlations between Σ_z and L was also confirmed.

The data points for the correlation (7.8) are shown in Figure 9, with the recommended fit,

$$\Sigma_z / L_B = [0.32(x/L_B)^{\frac{1}{2}} + 0.19]^2 \tag{7.9}$$

In determining the fit, the 1984 results were given more weight, since the temperature sensing grid was not high enough in much of the 1983 data.

Eq. (7.9) can be interpreted as showing that vertical dispersion depends on both atmospheric and buoyancy induced mixing, by rewriting it as,

$$\Sigma_z = [(0.10x)^{\frac{1}{2}} + (0.036L_B)^{\frac{1}{2}}]^2 \tag{7.10}$$

With no burners operating, ($L_B = 0$)

$$\Sigma_z(x) = 0.10x \tag{7.11}$$

which is in good agreement with the Pasquill-Gifford curves for the vertical dispersion parameter σ_z, for weather categories B and C; see Turner (1970), Beychok (1979). Assuming this equivalence, (7.10) may be rewritten as,

$$\Sigma_z = [\sigma_z^{\frac{1}{2}} + (0.036L_B)^{\frac{1}{2}}]^2 \tag{7.12}$$

8. WATER FLUME STUDIES

Coincident with the CRNL field tests, a similar study was carried out under contract to AECL in the water flume (W/F) facility of the University of Waterloo; see Slawson (1986). The source was provided by an array of small ($\simeq$ 2 mm) jets arranged in various geometries with dimensions between 0.1 m and 0.3 m, approximately, which injected a buoyant heated dye from a manifold mounted beneath the floor of the flume. A combination of photography and temperature measurement was used to observe the downstream plume. The purpose of the W/F study was to provide a more controlled environment, where the characteristic behaviour and scalability of certain features, particularly plume lift-off and centreline trajectory, could be determined. Plume parameters were obtained by fitting observed plume cross-sections to equivalent ellipses and correlating the semi-minor axis and centrelines with buoyancy and source parameters.

The W/F results show very clearly the difference in the two sets of experimental conditions. In the W/F, unlike the atmosphere, there is relatively little ambient mixing, and the main driving force for plume rise and spread is buoyancy. The plume parameters were therefore correlated differently in the two cases. Nevertheless, the W/F work provided considerable help in interpreting the CRNL data. Specifically, it identified the importance of the initial jet momentum, which could be more clearly observed, although it was handled somewhat differently in the analysis; see Slawson (1986). It also identified clearly the "lift-off distance" downwind of the source, which could not be directly observed in the CRNL tests. Slawson's data for x_L is shown in Figure 10. The improvement in the centreline correlation of the CRNL data resulting from the use of Eq. (6.5) is, however, confirmation that the phenomenon exists at larger scale and has been determined with reasonable accuracy. Most important, the centreline correlation $z_c(x,L_B,F)$ was found to be in good agreement between the two sets of experiments. The best agreement was obtained with ground-based line sources. Figure 11 shows the data points from Fig. (3.22) of Slawson (1986) with the correlation Eq. (6.10) for comparison, for ground-based line sources. The disagreement is due to differences in accounting for jet momentum, and may be partly due to the different levels of ambient turbulence in the two sets of experiments, as already noted. The good agreement of the plume centreline trajectories shows that it depends principally on buoyancy, and less on ambient mixing. The agreement is encouraging because it demonstrates the inherent scalability of this parameter over a wide range of source dimensions, and a realistic correlation with source parameters.

9. SUMMARY

Extensive plume temperature measurements have been interpreted to identify and correlate the most important parameters of a ground-based plume blown over in a cross-wind. The effect of initial jet momentum, clearly discernible in the more accurately controlled water flume environment, has been analysed in terms of burner properties. The lift-off length of the plume, obtained from the water flume studies of Slawson (1986), has been used in deriving a satisfactory correlation of the elevated plume centreline trajectory. The trajectory is strongly dependent on source and buoyancy parameters, and is based on source sizes between 0.1 m and 4.0 m. Lateral (cross-wind) dispersion depends on source diameter L and on atmospheric dispersion through $\sigma_y(x)$, but is uncorrelated with buoyancy. Vertical dispersion depends on buoyancy through L_B and on atmospheric dispersion through σ_z, but is uncorrelated with source dimension L. Conservation of plume energy, allowing a radiation loss of 10 to 15%, appears to be confirmed, although with considerable scatter. The description of Σ_z is less satisfactory than that of Σ_y and z_c, since there appears to be some residual vertical skewness, perhaps due to wind shear or other ground effects, or to near-source effects on the wind profile. It does, however, describe the temperature peak accurately down to about one-half the peak value.

The overall correlation of temperature rise, using the standard Gaussian model with modified dispersion and plume rise parameters as derived, is in a form that gives confidence it correctly includes the most important physical effects and can, therefore, be applied to sources of much larger scale.

REFERENCES

Beychok, M.R., "Fundamentals of Stack Gas Dispersion", published by M.R. Beychok, 63 Oak Tree Lane, Irvine, CA 92715 (1979).

Briggs, G.A., "Plume Rise", AEC Critical Review Series, USAEC Division of Technical Information, Oak Ridge, TENN (1969).

Dilworth, Secord, Meagher and Associates (DSMA), Report No. 653/797, "Glace Bay Heavy Water Plant GDS Performance", submitted to AECL (1975).

Morton, B.R., Taylor, Sir G.I., and Turner, J.S., "Turbulent Gravitational Convection from Maintained and Instantaneous Sources", Proc. Royal Society Vol. A234, pp 1-23 (1956).

Pasquill, F., "Atmospheric Diffusion", 2nd ed., J. Wiley and Sons, New York (1974).

Rankine, A.O., "Experimental Studies in Thermal Convection", Proc. Phys. Soc., Vol. A63, pp 417-443, (1950).

Rouse, H., "Gravitational Diffusion from a Boundary Source in Two-Dimensional Flow", ASME Jl. of Appl. Mech., Vol. 14, No. 3, pp A225-228 (1947).

Selander, W.N., unpublished AECL report (1977).

Selander, W.N., unpublished AECL report (1978).

Slawson, P., "On the Behaviour of Buoyant Line Sources of Heat Near Ground Level", submitted to AECL (1976).

Slawson, P., "Laboratory Simulation and Mathematical Modelling to Assist in the Performance Evaluation of GDS", submitted to AECL (1986).

Thomas, P.H., "The Effect of Wind on Plumes from a Line Heat Source", U.K. Dept. of Scientific and Industrial Research, Fire Research Note No. 572 (unpublished report), (1964).

Turner, D.B., "Workbook of Atmospheric Dispersion Estimates", U.S. Dept. of Health, Education and Welfare (1970).

11. ACKNOWLEDGEMENTS

The authors wish to acknowledge the many helpful consultations with Professor P.R. Slawson of the University of Waterloo, and to thank the following people:

George Whittle, who wired the thermocouple array and connected it to the data logger;

Frank Brown and Don Wildsmith, who provided techical assistance in the field and managed the data gathering process;

Vickie Ruddock, who did the subsequent data handling and wrote the computer programs for smoothing and fitting the data; and

Joanne Evraire, who typed the final version of the report.

Test-Time	Date	Geom.	LC (m)	N	QQ (MW)	TO (°C)	UJ (m/s)	U* (m/s)	ZO (cm)
1C6232-0853	83/08/20	C	1.0	6	.132	21.6	17.2	.393	2.0
1C6232-0903	"	C	1.0	6	.132	21.7	17.2	.455	2.0
2C4232-0949	"	C	1.0	4	.132	22.2	17.2	.386	2.0
3C8232-1029	"	C	1.0	8	.132	22.4	17.2	.361	2.0
3C8232-1038	"	C	1.0	8	.132	22.4	17.2	.431	2.0
4C9232-1239	"	C	1.0	9	.132	21.6	17.2	.446	2.0
4C9232-1249	"	C	1.0	9	.132	21.7	17.2	.497	2.0
5C9235-0827	83/08/23	C	1.0	9	.132	16.8	17.2	.176	2.0
6C6235-0915	"	C	1.0	5	.132	18.0	17.2	.202	2.0
7C4235-1009	"	C	1.0	4	.132	19.0	17.2	.207	2.0
7C4235-1019	"	C	1.0	4	.132	19.1	17.2	.209	2.0
8C3235-1326	"	C	1.0	3	.173	21.8	19.9	.223	2.0
8C3235-1336	"	C	1.0	3	.173	21.9	19.9	.255	2.0
1C4251-1415	83/09/08	C	1.0	4	.162	22.9	19.2	.247	2.0
1C4251-1425	"	C	1.0	4	.162	22.9	19.2	.217	2.0
1C6256-1351	83/09/13	C	1.0	6	.173	14.4	19.9	.168	2.0
116284-1330	83/10/11	C	2.0	16	.132	17.4	17.2	.275	1.3
116284-1341	"	C	2.0	16	.132	17.5	17.2	.293	1.3
116284-1351	"	C	2.0	16	.132	17.5	17.2	.278	1.3
208284-1413	"	C	2.0	8	.132	17.4	17.2	.301	1.3
208284-1425	"	C	2.0	8	.132	17.5	17.2	.275	1.3
312284-1632	"	C	2.0	12	.132	15.5	17.2	.232	1.3
404284-1700	"	C	2.0	4	.132	14.4	17.2	.244	1.3
404284-1710	"	C	2.0	4	.132	14.2	17.2	.244	1.3
112285-1614	83/10/12	C	2.0	12	.173	13.1	19.9	.291	1.3
112285-1624	"	C	2.0	12	.173	13.1	19.9	.272	1.3
206285-1638	"	C	2.0	6	.173	13.2	19.9	.257	1.3
206285-1649	"	C	2.0	6	.173	13.4	19.9	.276	1.3
316285-1704	"	C	2.0	16	.173	13.5	19.9	.290	1.3
316285-1714	"	C	2.0	16	.173	13.2	19.9	.272	1.3
112288-1143	83/10/15	C	2.0	12	.173	6.5	19.9	.324	1.5
216288-1221	"	C	2.0	16	.132	7.0	17.2	.206	1.5
216288-1231	"	C	2.0	16	.132	7.8	17.2	.294	1.5
104299-1635	83/10/26	P	-	4	.132	3.4	17.2	.143	1.5
214299-1653	"	DL	2.5	14	.132	3.5	17.2	.128	1.5
214299-1701	"	DL	2.5	14	.132	3.5	17.2	.146	1.5
214300-0944	83/10/27	DL	2.5	14	.132	4.8	17.2	.291	1.5
214300-1002	"	DL*	2.5	14	.132	4.2	17.2	.305	1.5
214300-1013	"	DL*	2.5	14	.132	4.6	17.2	.345	1.5
314300-1031	"	DL**	2.5	14	.132	5.1	17.2	.323	1.5
314300-1042	"	DL**	2.5	14	.132	5.0	17.2	.331	1.5
314300-1053	"	DL**	2.5	14	.132	5.1	17.2	.331	1.5
414300-1301	"	DL***	2.5	14	.132	8.2	17.2	.275	1.5
414300-1313	"	DL***	2.5	14	.132	7.6	17.2	.245	1.5
504300-1336	"	P	-	4	.132	7.2	17.2	.261	1.5
504300-1348	"	P	-	4	.132	6.7	17.2	.270	1.5

* DL with lines 50 cm apart
** DL with lines 100 cm apart
*** DL with lines 150 cm apart

TABLE 2

Compilation of 1984 Tests (46 Cases)

Test-Time	Date	Geom.	LO (m)	N	QO (MW)	TO (°C)	Uj (m/s)	L* (m/s)	ZO (cm)
2C9229-1502	84/08/16	L	6.8	9	.132	19.9	17.2	.258	1.0
2C9229-1512	"	L	6.8	9	.132	19.2	17.2	.319	1.0
3C9229-1527	"	L	6.8	9	.173	18.5	19.9	.252	1.0
3C9229-1539	"	L	6.8	9	.173	18.0	19.9	.212	1.0
419229-1556	"	L	6.8	19	.173	17.7	19.9	.202	1.0
119236-0900	84/08/23	L	6.8	19	.132	13.3	17.2	.302	1.0
119236-0912	"	L	6.8	19	.132	13.1	17.2	.278	1.0
210236-0928	"	L	6.8	10	.132	12.9	17.2	.268	1.0
104265-1250	84/09/21	P	-	4	.132	14.2	17.2	.312	1.0
308265-1343	"	C	1.0	8	.132	15.2	17.2	.292	1.0
408265-1411	"	C	2.0	8	.132	15.3	17.2	.276	1.0
516265-1436	"	C	2.0	16	.132	16.0	17.2	.312	1.0
516265-1448	"	C	2.0	16	.132	15.8	17.2	.277	1.0
616265-1503	"	C	2.0	16	.173	15.5	19.9	.246	1.0
704265-1700	"	P	-	4	.173	15.1	19.9	.248	1.0
704265-1712	"	P	-	4	.173	14.9	19.9	.243	1.0
804265-1726	"	P	-	4	.132	14.4	17.2	.248	1.0
804265-1738	"	P	-	4	.132	14.5	17.2	.233	1.0
104270-0845	84/09/26	P	-	4	.132	3.7	17.2	.293	1.0
104270-0855	"	P	-	4	.132	4.3	17.2	.309	1.0
104270-0905	"	P	-	4	.132	4.1	17.2	.332	1.0
216270-0934	"	C	3.0	16	.132	2.6	17.2	.236	1.0
216270-0944	"	C	3.0	16	.132	2.5	17.2	.295	1.0
216270-0954	"	C	3.0	16	.132	4.0	17.2	.288	1.0
326270-1031	"	C	3.0	26	.125	4.5	16.7	.304	1.0
406270-1349	"	P	-	6	.132	5.8	17.2	.296	1.0
406270-1359	"	P	-	6	.132	5.5	17.2	.295	1.0
508270-1414	"	P	-	8	.132	5.8	17.2	.290	1.0
508270-1424	"	P	-	8	.132	6.0	17.2	.256	1.0
610270-1436	"	P	-	10	.132	6.1	17.2	.225	1.0
610270-1446	"	P	-	10	.132	5.9	17.2	.330	1.0
726270-1707	"	C	3.0	26	.132	6.2	17.2	.176	1.0
813270-1717	"	C	3.0	13	.132	6.3	17.2	.137	1.0
909270-1731	"	C	3.0	9	.127	6.1	16.9	.137	1.0
126278-0908	83/10/04	C	3.0	26	.132	2.9	17.2	.270	1.0
126278-0918	"	C	3.0	26	.132	3.5	17.2	.266	1.0
214278-0933	"	C	3.0	14	.132	3.7	17.2	.216	1.0
214278-0943	"	C	3.0	14	.132	2.9	17.2	.233	1.0
336278-1235	"	C	4.0	36	.132	8.5	17.2	.182	1.0
336278-1245	"	C	4.0	36	.132	7.5	17.2	.186	1.0
418278-1315	"	C	4.0	18	.132	9.0	17.2	.149	1.0
504278-1333	"	P	-	4	.132	9.0	17.2	.194	1.0
504278-1343	"	P	-	4	.132	9.1	17.2	.216	1.0
504278-1353	"	P	-	4	.132	9.4	17.2	.227	1.0
602278-1412	"	P	-	2	.132	9.3	17.2	.211	1.0
602278-1422	"	P	-	2	.132	9.2	17.2	.183	1.0

TABLE 3 Lateral Dispersion Parameters for 1983 1-metre Circle Tests

Test/Time	N	U_* (m/s)	θ (deg)	σ_y(2.5m)	σ_y(5.0m)	σ_y(7.5m)	σ_y(10m)	σ_y(12.5m)	σ_y(15m)	σ_y(25m)
106232/0853	6	.393	310	1.19	1.48	1.50	3.17	-	4.95	-
106232/0903	6	.459	305	1.09	1.73	1.67	3.76	-	-	-
204232/0949	4	.383	310	1.12	1.81	1.98	3.48	-	3.30	-
308232/1029	8	.361	305	1.36	2.23	2.37	3.30	-	3.00	-
308232/1038	8	.431	310	1.20	2.04	2.20	2.85	-	-	-
409232/1239	9	.440	315	1.08	1.87	2.25	3.37	-	4.16	6.59
409232/1249	9	.497	315	1.09	1.86	2.63	3.77	-	4.47	6.98
509235/0827	9	.176	305	1.42	2.55	3.51	-	-	-	-
606235/0915	6	.202	310	0.88	1.78	3.26	4.55	-	5.00	-
704235/1009	4	.207	305	1.17	1.66	2.21	4.45	-	-	-
704235/1019	4	.209	300	1.63	2.38	2.99	4.57	-	-	-
803235/1326	3	.223	305	1.28	2.06	2.46	4.38	-	-	-
803235/1336	3	.255	305	1.28	2.11	2.28	3.55	-	-	-
106235/1351	6	.168	310	1.38	2.12	2.37	3.73	4.35	-	-
104299/1635	4	.143	305	1.37	1.98	2.75	2.64	3.37	-	-
504300/1335	4	.270	300	1.15	1.85	2.64	3.38	3.55	-	-
Means				1.23	1.97	2.44	3.66	3.76	4.15	6.79
Standard Deviations				0.18	0.27	0.53	0.60	-	0.84	-

TABLE 4 Lateral Dispersion Parameters for 1983 2-metre Circle Tests

Test/Time	N	U_* (m/s)	θ (deg)	σ_y(2.5m)	σ_y(5.0m)	σ_y(7.5m)	σ_y(10m)	σ_y(12.5m)	σ_y(15m)	σ_y(25m)
116284/1330	16	.275	140	.93	1.96	3.06	3.79	4.73	-	-
116284/1341	16	.293	135	1.23	2.15	3.76	4.06	5.60	4.97	-
116284/1351	16	.278	115	1.21	1.94	3.12	3.17	4.72	4.22	-
208284/1413	8	.301	130	1.26	1.97	3.66	3.69	4.93	5.36	-
208284/1425	8	.275	125	1.09	2.07	3.29	3.47	4.57	5.53	-
312284/1632	12	.232	130	1.26	1.77	2.62	3.92	4.27	6.18	-
404284/1700	4	.244	130	1.04	1.61	2.65	3.46	5.03	6.05	-
404284/1710	4	.244	130	0.92	1.54	2.35	3.50	4.13	3.54	-
112285/1614	12	.291	120	1.29	1.95	2.67	3.07	3.92	5.29	-
112285/1624	12	.272	125	1.42	1.80	2.84	3.83	4.28	5.85	-
206285/1638	6	.257	130	1.02	1.71	2.56	3.16	4.06	4.55	-
206285/1649	6	.276	125	1.05	1.57	2.58	2.60	3.18	3.48	-
316285/1704	16	.290	130	1.28	1.70	3.04	3.39	5.03	5.28	-
316285/1714	16	.272	130	1.48	1.80	2.61	3.41	3.90	4.91	-
112288/1143	12	.324	295	1.57	2.59	3.25	3.66	4.22	4.60	-
216288/1221	16	.306	300	1.70	2.23	3.61	4.24	6.95	7.29	-
216288/1231	16	.294	295	1.54	2.26	3.36	3.48	4.67	5.23	-
Means				1.25	1.92	3.00	3.52	4.60	5.15	
Standard Deviations				0.23	0.28	0.43	0.40	0.82	0.97	

TABLE 5 Lateral Dispersion Parameters for 1984 Point Source Tests

Test/Time	N	U_* (m/s)	θ (deg)	σ_y(2.5m)	σ_y(5.0m)	σ_y(7.5m)	σ_y(10m)	σ_y(12.5m)	σ_y(15m)	σ_y(25m)
104265/1250	4	.312	310	1.09	1.66	2.03	2.72	3.98	5.31	-
704265/1700	4	.248	315	1.05	1.97	2.81	3.49	4.00	4.88	-
704265/1712	4	.243	320	0.95	2.00	2.71	3.75	4.22	4.81	-
804265/1726	4	.248	315	1.03	1.68	1.93	2.75	2.67	3.38	-
804265/1738	4	.233	315	0.79	1.73	2.26	2.79	2.98	3.63	-
104270/0845	4	.293	296	-	1.53	2.16	2.94	3.77	4.38	
104270/0855	4	.309	304	-	1.66	2.61	3.32	4.74	5.22	
104270/0905	4	.332	320	-	1.80	3.00	4.43	4.27	4.46	
406270/1349	6	.296	295	-	1.58	2.25	2.98	3.74	4.60	
406270/1359	6	.295	298	-	1.65	2.33	2.68	3.61	3.88	
508270/1414	8	.290	300	-	1.67	2.35	2.74	3.36	3.73	
508270/1424	8	.256	295	-	1.91	2.83	3.74	4.80	4.85	
610270/1436	10	.225	305	-	1.92	2.77	3.33	4.61	4.94	
610270/1446	10	.330	305	-	1.89	2.64	3.37	3.52	3.81	
504278/1333	4	.194	300	-	2.21	3.50	4.08	5.81	-	
504278/1343	4	.216	300	-	2.07	3.53	3.78	4.70	-	
504278/1353	4	.227	300	-	1.91	2.30	2.50	3.50	-	
602278/1412	2	.211	305	-	2.22	3.04	4.44	5.25	-	
602278/1422	2	.183	310	-	2.63	-	4.71	-	-	
Means				0.98	1.88	2.61	3.40	4.09	4.42	
Standard Deviations				0.13	0.27	0.45	0.68	0.80	.062	

TABLE 6 Lateral Dispersion Parameters for 1984 2-metre Circle Tests

Test/Time	N	U_* (m/s)	θ (deg)	σ_y(2.5m)	σ_y(5.0m)	σ_y(7.5m)	σ_y(10m)	σ_y(12.5m)	σ_y(15m)	σ_y(25m)
408265/1411	8	.276	300	0.83	1.95	3.02	3.07	4.44	6.54	-
516265/1436	16	.312	310	0.93	2.00	3.10	3.68	4.81	5.65	-
516265/1448	16	.277	308	0.86	2.06	3.05	3.49	4.29	6.57	-
616265/1503	16	.246	310	0.93	2.19	2.98	3.46	3.99	4.60	-
Means				0.89	2.05	3.04	3.43	4.38	5.84	
Standard Deviations				0.06	0.10	0.05	0.26	0.34	0.93	

TABLE 7 Lateral Dispersion Parameters for 1984 3-metre Circle Tests

Test/Time	N	U_* (m/s)	θ (deg)	σ_y(2.5m)	σ_y(5.0m)	σ_y(7.5m)	σ_y(10m)	σ_y(12.5m)	σ_y(15m)	σ_y(25m)
216270/0934	16	.236	323	-	1.85	3.17	3.95	4.25	4.45	-
216270/0944	16	.295	317	-	2.00	3.31	4.30	4.82	5.66	-
216270/0954	16	.288	310	-	1.60	2.41	3.31	3.61	4.25	-
326270/1031	26	.304	310	-	2.33	3.36	4.20	5.45	6.98	-
726270/1707	26	.176	290	-	2.37	3.93	3.94	4.63	5.08	-
813270/1717	13	.137	290	-	2.15	3.44	3.68	4.53	5.70	-
909270/1731	9	.137	290	-	1.97	3.63	4.38	5.05	6.64	-
126278/0908	26	.270	305	-	2.34	3.32	3.92	4.74	5.17	-
126278/0918	26	.266	315	-	1.98	2.91	3.87	4.65	5.46	-
214278/0933	14	.216	310	-	1.81	2.69	3.44	4.21	4.37	-
214278/0943	14	.233	300	-	1.82	2.41	3.08	3.81	3.85	-
Means					2.02	3.14	3.82	4.52	5.24	
Standard Deviations					0.26	0.49	0.41	0.53	0.96	

TABLE 8 Lateral Dispersion Parameters for 1984 4-metre Circle Tests

Test/Time	N	U* (m/s)	θ (deg)	σ_y(2.5 m)	σ_y(5.0 m)	σ_y(7.5 m)	σ_y(10 m)	σ_y(12.5 m)	σ_y(15 m)	σ_y(25 m)
336278/1235	36	0.186	295	-	2.12	3.22	3.49	4.41	5.26	-
336278/1245	36	0.182	300	-	2.08	3.34	3.83	4.98	5.21	
			Means		2.10	3.28	3.66	4.70	5.24	

TABLE 9 Lateral Dispersion Parameters - Overall Mean and Standard Deviations

Downwind Distance	(m)	2.5	5.0	7.5	10.0	12.5	15.0	25.0
Mean σ_y	(m)	1.18	1.95	2.8	3.57	4.36	4.92	6.79
Standard Deviation	(m)	0.22	0.26	0.52	0.53	0.75	0.96	-

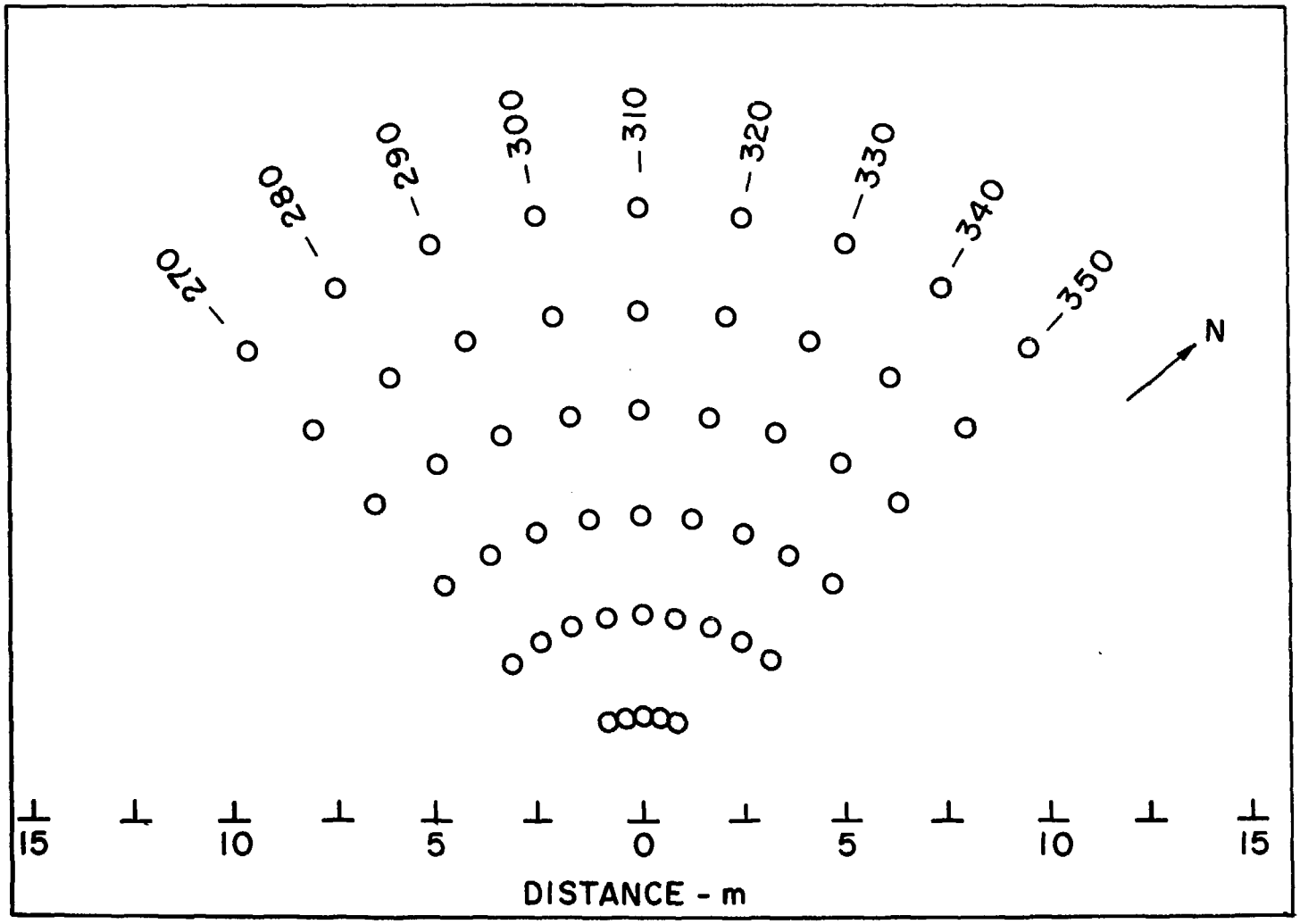

FIGURE 1a: Plan View of Thermocouple Mounting Poles Showing Prevailing Wind Direction with Heat Source at Centre

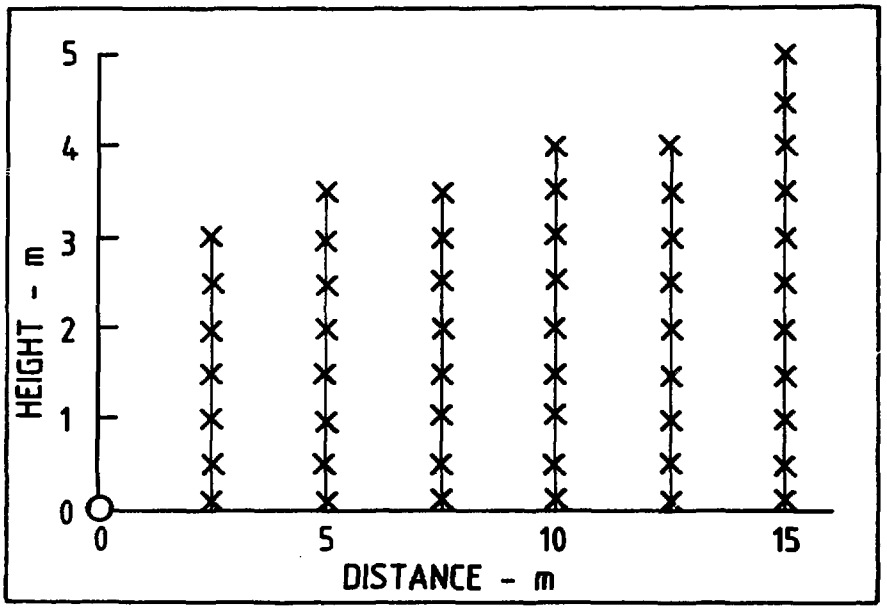

FIGURE 1b: Elevation View of Thermocouple Mounting Poles (Horizontal and Vertical Scales Unequal)

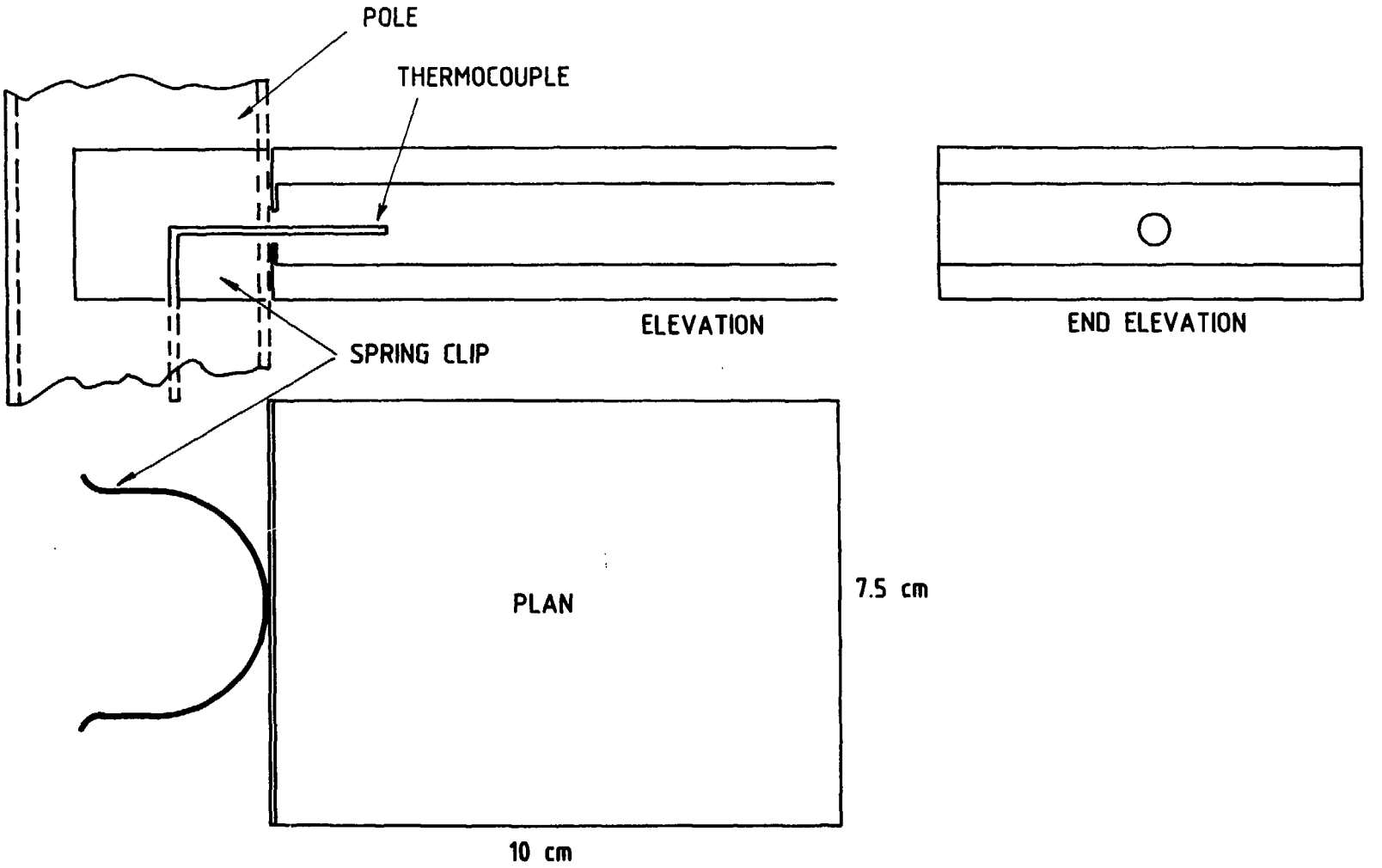

FIGURE 2: Plan and Elevation Views of Radiation Shield

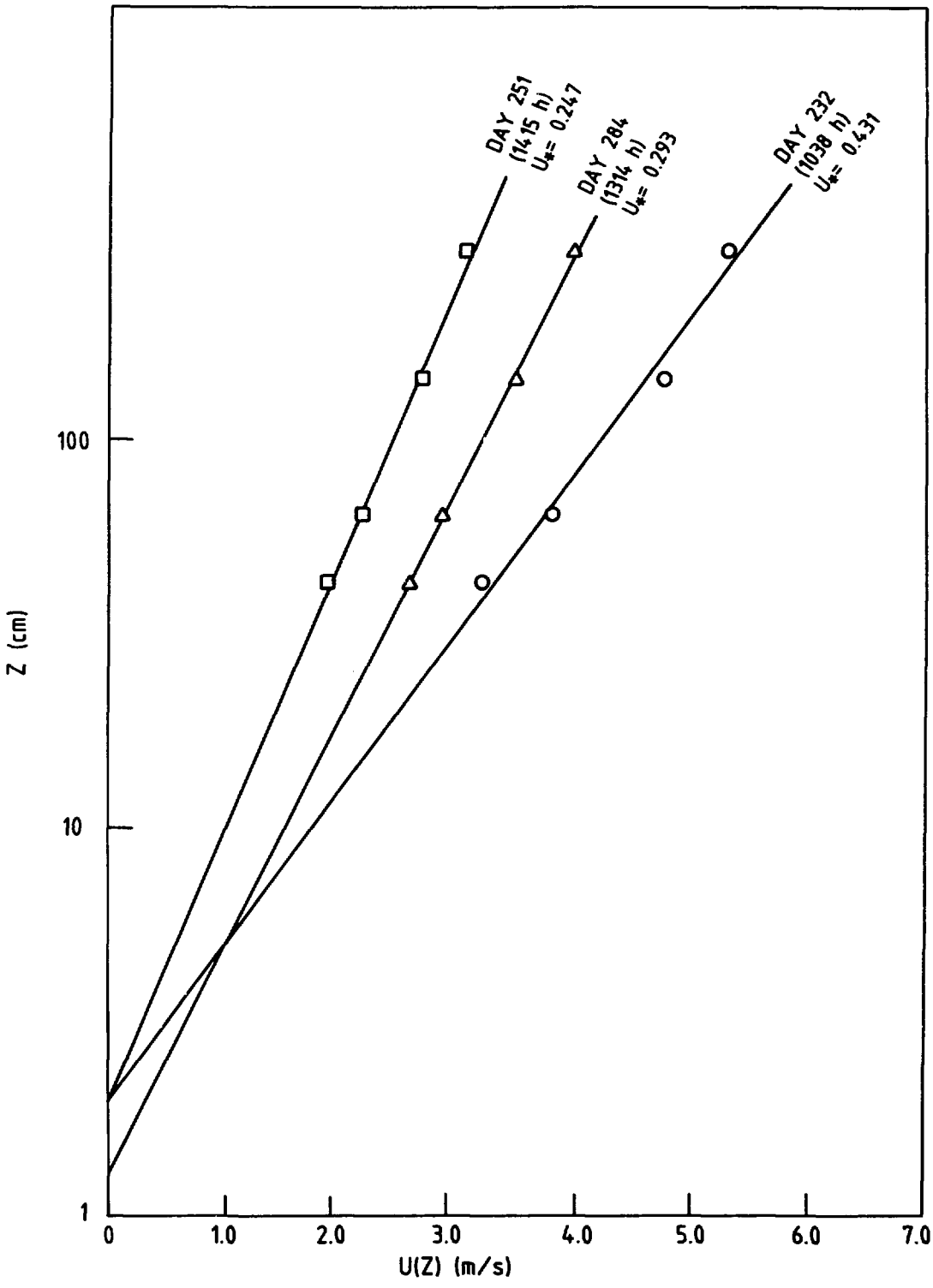

FIGURE 3: Typical Wind Profiles - 1983 Data

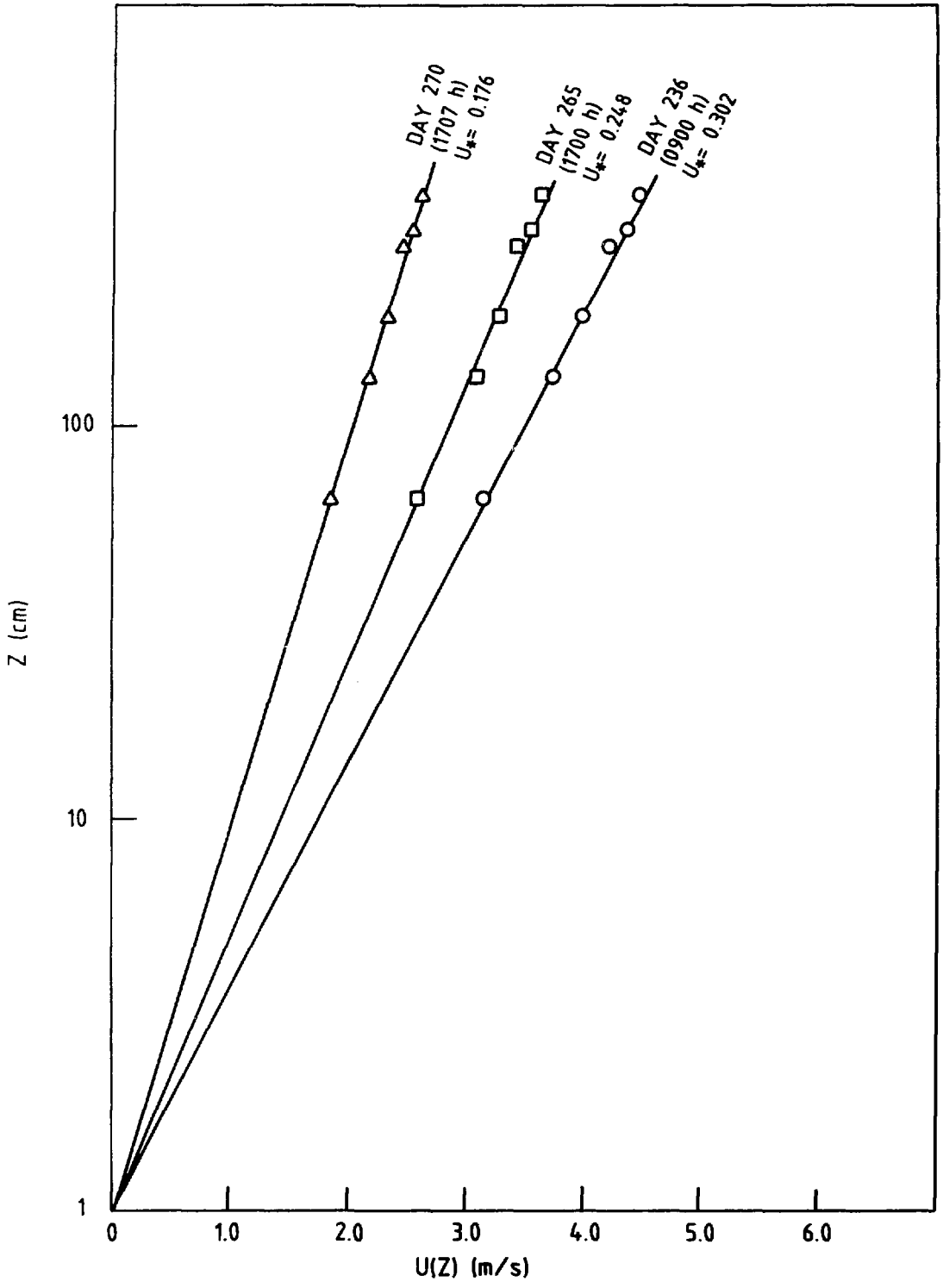

FIGURE 4: Typical Wind Profiles - 1984 Data

Compass bearing degrees	340	330	320	310	300	290	280	270	260	
3.0	0.00	0.00	18.78	51.27	52.22	34.93	0.00	0.00	0.00	
Sensor 2.5	0.00	0.00	20.64	54.78	54.35	35.02	18.90	0.00	0.00	
height 2.0	0.00	0.00	26.89	54.55	23.97	21.51	19.20	0.00	0.00	Line no. 1
(metres) 1.5	0.00	0.00	43.23	44.23	37.04	29.86	24.57	0.00	0.00	(2.5 m)
1.0	0.00	0.00	69.65	67.95	56.20	46.85	35.38	0.00	0.00	
.5	0.00	0.00	52.74	51.87	65.81	40.12	32.23	0.00	0.00	
.1	0.00	0.00	22.81	24.44	20.47	19.79	18.97	0.00	0.00	
3.5	17.01	16.55	18.96	16.42	18.27	15.45	15.08	14.85	14.56	
3.0	16.05	17.93	17.95	19.10	18.36	16.50	14.89	14.78	14.70	
2.5	17.62	19.66	20.93	21.60	20.14	18.29	15.99	15.99	15.16	Line no. 2
2.0	16.34	21.65	22.86	25.61	24.99	19.96	18.08	18.69	16.99	(5.0 m)
1.5	18.14	23.25	27.83	30.32	27.94	22.63	18.91	17.50	17.18	
1.0	18.93	23.00	29.61	30.43	30.44	23.40	19.26	16.04	16.39	
.5	17.50	21.00	23.90	24.47	24.73	21.66	18.50	17.05	16.57	
.1	18.77	19.83	19.88	20.19	19.12	19.47	19.20	18.01	17.71	
3.5	14.80	17.34	16.61	18.20	18.10	15.54	14.39	14.73	14.43	
3.0	15.03	17.32	19.03	18.17	17.30	15.89	15.22	15.20	14.03	
2.5	15.12	18.01	19.14	20.41	16.40	16.50	15.59	15.36	14.25	Line no. 3
2.0	15.31	17.70	18.87	21.28	19.20	17.40	16.27	15.60	15.25	(7.5 m)
1.5	16.28	18.50	20.03	21.51	20.41	17.72	16.28	15.40	15.40	
1.0	16.74	18.72	19.37	21.67	20.15	17.73	15.99	15.67	15.52	
.5	16.76	18.44	18.34	20.25	18.22	17.28	16.50	15.87	15.83	
.1	18.01	19.41	18.11	19.40	18.17	18.78	17.43	17.08	17.53	
4.0	14.87	14.84	16.44	16.42	17.33	15.27	15.44	14.99	14.66	
3.5	14.84	15.18	17.41	17.16	16.74	16.32	15.31	14.99	14.43	
3.0	15.09	16.05	17.88	18.20	17.00	16.67	15.60	14.96	14.36	Line no. 4
2.5	15.04	16.47	17.90	18.05	17.75	17.29	15.42	15.01	14.61	(10.0 m)
2.0	15.06	16.15	18.67	19.15	17.80	17.01	15.57	15.52	15.88	
1.5	15.39	16.59	18.62	19.17	18.90	16.57	15.61	15.58	14.93	
1.0	16.29	16.61	18.01	19.50	18.86	16.87	15.70	16.02	15.30	
.5	15.75	16.22	17.03	18.51	17.99	16.92	15.86	16.20	15.98	
.1	19.49	18.36	18.52	18.61	18.95	18.19	18.22	18.12	19.01	
4.0	14.82	16.12	16.92	16.37	16.88	15.23	14.84	14.18	14.27	
3.5	15.20	15.59	16.41	16.71	16.56	15.48	15.23	14.29	14.42	
3.0	15.78	18.93	16.80	17.14	17.16	15.73	15.37	14.55	14.56	Line no. 5
2.5	15.14	16.63	16.88	17.30	16.87	16.15	15.77	15.18	14.65	(12.5 m)
2.0	16.08	16.17	17.56	17.36	16.82	16.54	15.50	15.19	14.53	
1.5	15.38	15.62	17.32	17.16	17.19	16.32	15.49	16.74	14.70	
1.0	16.00	16.42	18.58	17.26	17.18	16.08	16.00	15.45	14.74	
.5	16.41	16.71	17.55	16.97	17.59	16.02	16.39	15.91	15.29	
.1	19.18	17.96	18.37	18.28	21.18	19.43	19.77	19.32	17.63	
5.0	15.43	15.18	15.53	15.30	14.95	15.85	13.52	14.57	15.34	
4.5	14.78	14.96	15.46	15.30	14.76	15.70	14.17	14.48	15.17	
4.0	16.06	15.47	15.95	15.50	15.09	15.52	14.84	15.56	15.20	Line no. 6
3.5	15.43	14.63	15.74	15.81	15.27	15.79	14.43	14.86	15.36	(15.0 m)
3.0	15.80	15.11	16.35	15.86	15.34	15.83	15.71	14.97	14.67	
2.5	15.93	15.00	15.22	17.51	15.39	15.13	15.37	14.09	14.73	
2.0	15.66	15.70	15.86	15.60	15.40	15.20	15.00	14.16	14.37	
1.5	16.53	15.22	15.87	16.29	15.30	15.00	14.75	14.31	15.33	
1.0	15.96	16.48	16.41	15.33	15.17	15.30	15.55	14.47	15.99	
.5	17.97	16.85	16.36	16.59	17.84	16.50	15.64	15.31	16.02	
.1	19.16	18.27	18.30	18.31	17.90	16.80	17.12	16.62	17.38	

Calendar Day/Time: 265/1250

No. of Burners, N = 4

Nominal Burner Power, Q = 0.130 MW

Circle Diameter, L = 0.5 m

Ambient Temperature, T_0 = 14.2°C

FIGURE 5(a): 10-Minute Temperature Means (1984)

Compass bearing degrees		340	330	320	310	300	290	280	270	260	
	3.0	0.00	0.00	22.03	72.54	76.39	51.50	0.00	0.00	0.00	
	2.5	0.00	0.00	32.44	77.32	67.77	51.38	24.13	0.00	0.00	
Sensor	2.0	0.00	0.00	38.35	72.90	35.42	33.17	29.30	0.00	0.00	Line no. 1
height	1.5	0.00	0.00	62.61	66.61	58.04	53.66	44.42	0.00	0.00	(2.5 m)
(metres)	1.0	0.00	0.00	96.83	107.66	97.68	84.62	71.03	0.00	0.00	
	.5	0.00	0.00	72.72	88.66	80.00	76.87	62.10	0.00	0.00	
	.1	0.00	0.00	27.35	28.41	25.05	24.32	22.70	0.00	0.00	
	3.5	19.86	20.45	25.23	19.78	23.81	19.60	17.47	17.47	16.44	
	3.0	19.34	22.61	22.69	23.46	25.88	22.51	19.12	17.87	16.71	
	2.5	22.33	25.15	26.05	28.22	27.56	25.42	22.51	19.19	18.69	Line no. 2
	2.0	22.20	28.19	29.07	32.39	33.63	30.99	28.23	23.08	19.09	(5.0 m)
	1.5	21.99	29.28	35.15	40.74	38.65	32.86	30.09	24.50	20.13	
	1.0	24.21	27.50	36.70	40.61	37.68	31.64	31.51	24.64	19.35	
	.5	20.17	25.00	29.72	30.15	29.98	26.20	24.19	21.83	19.17	
	.1	20.52	22.00	22.15	22.59	22.27	22.03	20.67	19.81	19.77	
	3.5	17.13	20.39	19.89	20.78	23.14	19.45	17.01	16.76	16.16	
	3.0	17.33	20.68	22.14	21.00	21.50	20.90	18.54	17.51	15.95	
	2.5	17.61	21.77	23.89	20.36	20.10	21.00	19.83	18.06	16.00	Line no. 3
	2.0	17.57	21.18	23.53	27.20	24.36	23.46	20.92	18.77	16.67	(7.5 m)
	1.5	18.33	21.51	23.91	26.72	24.05	23.43	21.61	18.92	17.00	
	1.0	18.72	21.17	23.09	25.04	22.32	21.86	20.38	18.37	17.43	
	.5	18.26	19.70	20.44	22.48	19.81	19.64	19.80	18.28	17.68	
	.1	19.51	20.89	19.84	21.16	19.80	20.60	19.29	18.88	19.34	
	4.0	16.41	16.82	18.36	18.22	20.39	18.57	17.52	16.43	16.20	
	3.5	16.71	17.26	20.04	19.04	20.01	19.99	18.02	16.28	15.93	
	3.0	16.98	17.76	20.77	20.41	20.51	20.67	18.50	16.62	15.67	Line no. 4
	2.5	17.01	18.70	21.01	21.05	21.31	21.41	18.47	17.02	15.64	(10.0 m)
	2.0	16.93	18.36	21.77	22.21	20.78	20.77	18.67	17.55	17.17	
	1.5	17.06	18.81	21.92	21.70	20.81	19.88	18.60	17.51	16.40	
	1.0	17.78	18.40	20.79	21.64	20.47	19.67	18.20	17.62	16.76	
	.5	16.98	17.53	18.73	20.17	19.41	18.98	17.61	17.50	17.44	
	.1	21.06	19.60	20.05	19.88	20.38	19.62	19.72	19.68	20.61	
	4.0	16.23	18.37	19.46	18.01	19.09	17.64	16.87	15.72	15.24	
	3.5	16.73	17.54	18.60	18.15	19.07	18.12	17.10	15.71	15.46	
	3.0	17.67	15.74	19.44	18.71	19.56	18.41	17.39	15.95	15.71	Line no. 5
	2.5	16.79	18.81	19.38	19.50	18.83	18.38	17.84	16.46	15.75	(12.5 m)
	2.0	17.75	18.09	20.00	19.59	18.62	18.49	17.61	16.61	15.58	
	1.5	16.78	17.24	19.11	18.88	18.77	18.31	17.41	19.20	15.78	
	1.0	17.00	17.86	20.34	18.36	18.40	18.26	17.50	17.08	15.86	
	.5	17.45	17.86	19.01	17.67	18.99	17.88	17.66	17.13	16.55	
	.1	20.33	19.22	20.01	19.04	22.37	20.91	19.64	19.17	19.72	
	5.0	16.71	16.47	17.16	17.00	16.73	17.74	14.70	15.66	16.43	
	4.5	15.80	16.36	17.23	17.50	16.42	17.60	15.55	15.80	16.25	
	4.0	17.46	17.01	18.31	17.80	17.12	17.53	15.94	16.66	16.30	Line no. 6
	3.5	16.54	15.86	18.15	17.36	17.26	17.72	16.02	15.60	16.33	(15.0 m)
	3.0	16.94	16.58	19.28	17.66	17.52	17.70	17.30	17.91	15.52	
	2.5	17.30	16.42	17.68	19.45	17.74	17.00	16.57	15.10	15.51	
	2.0	17.05	82.53	18.46	37.39	17.50	17.00	16.56	15.11	15.28	
	1.5	18.16	16.23	18.26	17.93	17.31	17.00	16.48	15.32	16.13	
	1.0	17.12	17.66	18.34	17.80	16.73	16.80	16.91	15.65	17.08	
	.5	19.29	17.80	17.71	17.65	16.49	16.80	17.00	16.86	17.04	
	.1	20.39	19.48	19.40	19.31	19.00	18.60	18.19	18.01	18.42	

Calendar Day/Time: 265/1343

No. of Burners, N = 8

Nominal Burner Power, Q = 0.130 MW

Circle Diameter, L = 1.0 m

Ambient Temperature, T_0 = 15.2°C

FIGURE 5(b): 10-Minute Temperature Means (1984)

Compass bearing degrees	340	330	320	310	300	290	280	270	260	
3.0	0.00	0.00	22.18	86.39	100.75	55.36	25.00	0.00	0.00	
2.5	0.00	0.00	68.79	93.53	96.85	55.63	24.73	0.00	0.00	
Sensor 2.0	0.00	0.00	49.90	94.19	40.06	40.47	32.02	0.00	0.00	Line no. 1
height 1.5	0.00	0.00	93.30	88.35	77.67	79.14	66.36	0.00	0.00	(2.5 m)
(metres) 1.0	0.00	0.00	161.10	155.53	152.34	144.38	129.76	0.00	0.00	
.5	0.00	0.00	134.14	144.61	204.30	153.08	135.61	0.00	0.00	
.1	0.00	0.00	46.03	44.87	44.19	37.87	33.11	0.00	0.00	
3.5	22.83	26.53	35.33	24.48	24.52	22.41	20.04	18.40	16.71	
3.0	24.70	30.09	38.00	31.18	28.89	26.00	23.12	21.00	17.65	
2.5	30.65	36.80	40.05	39.69	38.32	33.33	28.44	23.39	26.60	Line no.2
2.0	32.15	42.03	43.83	46.71	53.05	44.65	36.49	28.84	22.78	(5.0 m)
1.5	32.73	43.83	56.08	58.81	62.43	52.38	43.34	30.00	23.47	
1.0	34.36	41.00	58.33	57.05	65.76	54.19	46.76	33.23	21.76	
.5	22.89	32.00	40.51	39.90	44.93	37.48	32.20	27.48	19.62	
.1	21.49	23.32	24.50	24.74	23.50	23.20	22.26	21.32	19.80	
3.5	21.02	26.00	26.89	27.71	31.07	22.33	20.00	18.49	17.00	
3.0	21.64	27.52	28.22	28.48	27.00	25.19	22.73	19.86	17.00	
2.5	22.55	29.21	31.02	28.79	25.35	28.00	24.75	20.72	17.00	Line no. 3
2.0	22.85	29.94	30.10	35.86	34.38	30.55	26.65	21.80	17.00	(7.5 m)
1.5	23.49	30.10	30.71	35.30	32.57	30.66	27.41	21.70	17.00	
1.0	23.17	27.97	28.78	32.85	29.84	27.41	24.70	20.61	17.00	
.5	20.14	22.72	23.79	24.14	23.07	22.58	20.50	18.68	18.24	
.1	19.75	21.26	20.76	21.69	20.90	21.06	20.14	19.24	19.77	
4.0	18.61	19.90	22.21	23.39	23.54	19.93	18.19	17.24	16.64	
3.5	19.29	20.56	23.91	24.48	23.91	21.92	18.82	17.55	16.26	
3.0	19.68	21.62	24.85	26.43	25.00	23.02	19.71	17.84	16.27	Line no. 4
2.5	19.85	23.25	24.73	26.74	26.20	24.50	21.38	18.87	16.72	(10.0 m)
2.0	19.62	23.31	24.55	27.41	25.78	24.40	22.18	19.30	18.56	
1.5	19.52	22.44	24.15	26.16	24.92	23.43	21.91	19.50	17.51	
1.0	19.66	21.25	22.81	25.15	22.95	22.01	20.50	19.14	17.37	
.5	17.92	18.73	20.08	21.45	20.63	20.51	19.36	18.22	17.75	
.1	20.79	19.79	20.19	20.44	20.66	20.02	20.12	20.01	20.28	
4.0	17.88	20.87	22.03	22.48	21.73	18.93	18.27	17.01	15.81	
3.5	18.26	20.30	21.32	22.81	21.96	19.49	18.73	17.40	15.95	
3.0	18.96	18.41	21.54	22.95	22.39	20.42	19.32	18.06	16.57	Line no. 5
2.5	18.12	22.37	21.47	22.97	22.25	20.57	20.26	18.69	16.51	(12.5 m)
2.0	19.07	21.26	21.52	22.02	21.37	20.36	19.90	17.94	16.52	
1.5	18.06	19.76	20.58	20.73	20.98	19.98	19.68	19.85	16.34	
1.0	17.90	19.21	21.06	19.49	19.69	19.42	18.60	17.72	16.45	
.5	17.67	18.53	19.21	18.22	19.32	18.56	18.41	17.47	16.98	
.1	19.91	19.07	19.61	19.53	20.85	20.15	19.75	20.41	20.76	
5.0	18.04	18.04	19.75	19.50	19.32	17.80	16.54	16.95	16.99	
4.5	17.14	18.07	19.50	19.30	19.21	18.00	17.11	17.09	17.06	
4.0	18.44	18.99	20.05	19.90	19.91	18.39	17.93	17.85	14.20	Line no. 6
3.5	18.09	17.81	19.83	19.50	20.56	19.06	17.53	17.31	17.08	(15.0 m)
3.0	18.27	18.24	20.46	18.80	20.53	19.27	17.62	18.90	16.23	
2.5	18.71	17.93	18.92	20.00	19.82	18.72	17.64	16.86	16.23	
2.0	18.13	17.70	19.17	25.89	19.20	18.00	17.50	16.32	15.93	
1.5	18.59	17.41	18.46	18.78	18.77	17.90	17.20	15.92	16.53	
1.0	17.37	18.28	18.21	18.00	17.72	17.50	17.27	16.14	17.33	
.5	18.97	18.09	17.56	17.65	17.74	17.50	17.25	17.25	16.87	
.1	19.99	19.41	19.30	19.25	19.00	18.70	18.42	18.17	18.17	

Calendar Day/Time: 265/1436

No. of Burners, N = 16

Nominal Burner Power, Q = 0.130 MW

Circle Diameter, L = 2.0 m

Ambient Temperature, T_0 = 16.0°C

FIGURE 5(c): 10-Minute Temperature Means (1984)

Compass bearing degrees	340	330	320	310	300	290	280	270	260	
3.0	0.00	0.00	0.00	0.00	0.00	0.00	0.00	0.00	0.00	
2.5	0.00	0.00	0.00	0.00	0.00	0.00	0.00	0.00	0.00	
Sensor 2.0	0.00	0.00	0.00	0.00	0.00	0.00	0.00	0.00	0.00	Line no. 1
height 1.5	0.00	0.00	0.00	0.00	0.00	0.00	0.00	0.00	0.00	(2.5 m)
(metres) 1.0	0.00	0.00	0.00	0.00	0.00	0.00	0.00	0.00	0.00	
.5	0.00	0.00	0.00	0.00	0.00	0.00	0.00	0.00	0.00	
.1	0.00	0.00	0.00	0.00	0.00	0.00	0.00	0.00	0.00	
3.5	17.92	19.24	27.60	16.33	12.70	10.74	5.57	5.34	2.62	
3.0	21.31	23.99	0.00	21.68	19.25	13.00	6.12	4.74	2.70	
2.5	27.75	32.39	30.79	29.96	26.55	17.18	8.02	5.09	3.42	Line no. 2
2.0	35.57	37.84	35.54	34.07	30.00	24.25	8.62	5.29	4.21	(5.0 m)
1.5	35.79	34.94	38.67	35.19	36.10	26.01	9.55	5.00	4.26	
1.0	30.52	31.00	34.27	30.84	32.21	21.45	6.91	4.92	3.30	
.5	10.97	14.00	19.42	17.26	15.06	9.88	4.99	5.52	3.68	
.1	7.61	9.16	9.30	9.42	6.11	5.77	4.70	6.05	4.83	
3.5	15.79	18.50	16.77	12.93	14.70	6.70	5.84	3.98	3.10	
3.0	15.89	20.48	15.98	14.47	12.60	7.41	5.96	4.04	3.07	
2.5	17.25	21.69	20.44	15.50	11.84	8.00	5.58	3.93	3.46	Line no. 3
2.0	18.09	22.14	19.90	16.15	17.10	8.84	5.22	3.71	3.52	(7.5 m)
1.5	16.56	19.34	18.64	15.88	14.01	7.69	4.98	3.75	3.60	
1.0	12.55	14.06	13.94	12.62	12.27	6.53	4.18	3.49	3.72	
.5	6.26	8.00	8.21	6.62	6.00	4.44	4.50	3.73	3.82	
.1	4.47	5.79	5.28	5.43	5.10	4.66	4.73	4.48	4.54	
4.0	11.18	13.40	12.40	9.23	8.73	5.53	4.56	4.10	3.90	
3.5	10.96	13.61	12.97	9.74	8.31	5.71	4.62	4.03	3.71	
3.0	11.21	14.27	13.58	10.15	8.40	5.68	4.92	3.72	4.02	Line no. 4
2.5	10.94	13.29	13.50	10.45	8.15	5.91	4.59	3.65	3.70	(10.0 m)
2.0	10.17	12.13	13.56	10.24	7.50	5.26	4.15	3.54	4.17	
1.5	9.23	9.36	11.56	10.37	6.78	4.56	4.17	3.80	3.95	
1.0	7.28	6.95	9.44	7.84	5.60	3.96	3.90	4.02	3.80	
.5	4.97	5.14	6.04	5.65	4.68	3.74	3.62	4.13	4.28	
.1	4.70	4.98	5.15	4.86	4.93	4.83	4.42	4.94	5.43	
4.0	8.13	10.71	11.40	7.86	6.65	4.37	4.15	3.74	2.69	
3.5	7.82	10.26	11.11	8.11	6.36	4.53	4.11	3.59	2.70	
3.0	7.90	10.00	11.40	8.28	6.02	4.48	4.00	3.36	2.85	Line no. 5
2.5	7.65	9.64	10.36	8.25	6.05	4.02	4.09	3.21	2.91	(12.5 m)
2.0	7.79	8.12	9.88	7.90	5.55	3.66	4.08	3.31	2.89	
1.5	6.29	6.83	8.65	7.33	4.98	3.66	3.90	3.85	3.41	
1.0	5.20	6.67	7.13	5.94	4.21	3.79	3.80	3.85	3.66	
.5	4.14	4.91	5.64	4.83	4.07	3.86	3.71	3.87	3.87	
.1	4.53	4.70	4.99	4.65	4.62	4.39	4.11	4.30	4.60	
5.0	6.88	9.02	7.40	6.00	4.50	3.47	2.99	3.16	2.69	
4.5	6.81	8.62	7.92	6.00	4.31	3.30	2.94	3.65	2.80	
4.0	6.51	8.35	8.06	6.20	4.19	3.17	2.80	3.70	2.80	Line no. 6
3.5	7.24	7.89	8.57	6.79	3.94	3.16	2.76	3.75	2.87	(15.0 m)
3.0	7.03	7.70	8.09	6.41	3.55	3.02	2.57	3.20	2.57	
2.5	6.93	6.97	7.52	6.02	3.59	3.01	2.68	2.65	2.65	
2.0	7.95	6.10	6.64	5.50	3.50	3.11	2.80	2.58	2.54	
1.5	5.24	5.28	5.64	5.00	3.34	3.51	2.67	2.59	2.82	
1.0	4.59	4.77	5.11	4.10	3.15	2.89	2.76	2.56	3.09	
.5	4.05	4.40	4.36	3.70	3.40	2.75	3.05	3.10	3.09	
.1	4.28	4.20	4.00	3.81	3.70	3.60	3.53	3.48	3.47	

Calendar Day/Time: 270/934

No. of Burners, N = 16

Nominal Burner Power, Q = 0.130 MW

Circle Diameter, L = 3.0 m

Ambient Temperature, T_0 = 2.6°C

FIGURE 5(d): 10-Minute Temperature Means (1984)

Compass bearing degrees	340	330	320	310	300	290	280	270	260	
3.0	0.00	0.00	0.00	0.00	0.00	0.00	0.00	0.00	0.00	
2.5	0.00	0.00	0.00	0.00	0.00	0.00	0.00	0.00	0.00	
Sensor 2.0	0.00	0.00	0.00	0.00	0.00	0.00	0.00	0.00	0.00	Line no. 1
height 1.5	0.00	0.00	0.00	0.00	0.00	0.00	0.00	0.00	0.00	(2.5 m)
(metres) 1.0	0.00	0.00	0.00	0.00	0.00	0.00	0.00	0.00	0.00	
.5	0.00	0.00	0.00	0.00	0.00	0.00	0.00	0.00	0.00	
.1	0.00	0.00	0.00	0.00	0.00	0.00	0.00	0.00	0.00	
3.5	19.62	23.61	31.90	25.30	35.97	37.91	34.79	31.57	21.55	
3.0	21.90	28.05	33.00	33.05	44.91	42.00	38.45	39.00	26.25	
2.5	22.61	34.09	37.54	42.55	54.39	54.45	41.42	45.70	30.52	Line no. 2
2.0	23.79	37.47	39.80	46.43	61.00	63.33	45.32	49.94	36.01	(5.0 m)
1.5	21.04	27.81	43.49	51.31	68.26	70.42	41.33	36.00	29.66	
1.0	22.55	20.17	38.87	39.86	56.17	53.38	27.27	32.90	22.17	
.5	12.75	14.19	20.86	20.17	24.03	23.92	14.84	15.54	10.98	
.1	10.68	10.39	12.58	13.08	10.53	12.66	10.74	12.14	7.68	
3.5	11.71	18.62	19.75	23.98	26.17	29.82	28.68	26.76	18.17	
3.0	10.89	18.42	18.51	25.14	26.00	30.11	30.46	29.94	18.98	
2.5	10.29	17.52	23.84	25.60	25.70	29.00	31.83	29.51	18.59	Line no. 3
2.0	10.53	16.65	19.03	25.44	25.07	28.55	29.77	26.63	17.88	(7.5 m)
1.5	10.49	16.49	16.37	23.54	19.40	23.97	25.65	22.63	14.00	
1.0	10.39	12.70	13.00	12.73	15.86	17.47	15.58	14.49	11.58	
.5	8.87	9.98	9.10	8.92	9.74	10.71	10.00	9.77	8.37	
.1	7.61	9.41	8.83	8.77	9.23	9.64	9.28	8.51	8.37	
4.0	7.46	9.52	11.90	14.97	23.47	22.30	21.45	17.66	12.77	
3.5	7.56	9.64	13.36	14.41	22.30	19.84	21.83	18.60	12.38	
3.0	7.94	8.55	13.62	14.45	30.09	18.65	20.83	18.06	11.33	Line no. 4
2.5	7.57	9.17	12.91	14.22	19.37	17.40	18.85	17.05	10.96	(10.0 m)
2.0	7.76	8.24	11.44	14.03	16.12	15.13	17.42	14.30	10.06	
1.5	7.04	7.78	9.72	12.11	12.32	12.73	14.61	12.12	9.07	
1.0	6.96	7.70	8.25	9.15	10.05	9.96	9.70	9.47	8.06	
.5	6.36	7.02	7.15	7.72	8.44	7.91	8.40	7.35	7.44	
.1	7.59	7.30	7.66	7.68	8.32	8.02	8.00	7.86	7.70	
4.0	6.61	8.81	11.38	12.61	16.41	16.37	15.53	13.40	8.63	
3.5	6.64	7.92	9.64	11.56	15.57	15.00	15.46	12.37	7.65	
3.0	7.06	6.08	9.27	11.21	13.61	13.19	14.64	12.13	7.99	Line no. 5
2.5	6.67	8.25	8.68	11.24	12.58	11.82	12.88	10.96	7.38	(12.5 m)
2.0	6.61	7.78	8.43	10.16	11.18	10.12	10.58	9.64	7.05	
1.5	6.35	7.16	7.59	8.48	9.59	9.22	8.99	9.10	6.93	
1.0	0.00	7.15	7.45	7.24	8.45	8.65	8.20	7.90	6.96	
.5	6.51	6.59	7.49	7.01	7.67	7.83	7.45	7.14	6.83	
.1	7.20	6.76	7.26	7.47	7.64	7.80	7.33	7.43	7.24	
5.0	6.80	8.18	8.25	9.60	11.89	12.46	12.38	11.55	9.08	
4.5	6.59	7.73	7.82	9.60	11.33	12.00	12.12	10.94	8.48	
4.0	6.51	7.66	7.91	9.50	11.55	11.17	11.70	10.71	8.00	Line no. 6
3.5	6.20	6.95	7.58	9.41	10.31	10.42	11.09	9.61	7.34	(15.0 m)
3.0	6.21	6.75	7.41	8.81	9.55	9.26	10.95	9.00	6.99	
2.5	6.17	6.05	6.58	8.79	9.30	8.70	9.53	8.07	6.58	
2.0	6.20	6.10	6.59	7.50	8.00	7.79	8.66	7.36	6.48	
1.5	6.31	6.06	6.22	6.97	7.06	7.62	7.67	6.89	6.39	
1.0	6.17	6.23	6.40	6.30	6.26	7.18	6.86	6.60	6.40	
.5	6.27	6.25	6.35	6.62	6.68	6.75	6.55	6.52	6.12	
.1	6.68	6.56	6.50	6.52	6.70	6.88	6.68	6.62	6.34	

Calendar Day/Time: 270/1707

No. of Burners, N = 26

Nominal Burner Power, Q = 0.130 MW

Circle Diameter, L = 3.0 m

Ambient Temperature, T_0 = 6.2°C

FIGURE 5(e): 10-Minute Temperature Means (1984)

Compass bearing degrees	340	330	320	310	300	290	280	270	260	
3.0	0.00	0.00	0.00	0.00	0.00	0.00	0.00	0.00	0.00	
2.5	0.00	0.00	0.00	0.00	0.00	0.00	0.00	0.00	0.00	
Sensor 2.0	0.00	0.00	0.00	0.00	0.00	0.00	0.00	0.00	0.00	Line no. 1
height 1.5	0.00	0.00	0.00	0.00	0.00	0.00	0.00	0.00	0.00	(2.5 m)
(metres) 1.0	0.00	0.00	0.00	0.00	0.00	0.00	0.00	0.00	0.00	
.5	0.00	0.00	0.00	0.00	0.00	0.00	0.00	0.00	0.00	
.1	0.00	0.00	0.00	0.00	0.00	0.00	0.00	0.00	0.00	
3.5	25.10	34.66	37.00	42.23	44.09	40.65	36.00	32.86	21.99	
3.0	27.13	45.25	48.00	52.58	57.84	55.00	54.32	44.58	28.43	
2.5	38.09	55.48	65.11	73.90	73.53	67.77	60.21	58.04	35.28	Line no. 2
2.0	37.76	64.37	76.85	86.53	84.00	83.88	66.72	65.53	42.17	(5.0 m)
1.5	34.97	58.26	91.33	99.20	89.88	83.09	62.70	63.00	39.77	
1.0	30.67	52.00	83.71	86.90	71.57	66.07	42.93	59.19	30.30	
.5	12.69	26.00	35.13	41.58	36.04	31.90	17.67	22.75	15.21	
.1	14.76	15.38	17.39	19.19	18.02	18.48	13.10	14.33	11.07	
3.5	18.00	28.47	36.52	42.97	41.44	39.35	34.75	29.32	17.06	
3.0	18.36	28.73	35.75	42.08	40.00	42.57	37.97	34.58	16.50	
2.5	16.10	29.00	39.81	50.00	39.84	41.00	38.83	35.22	15.55	Line no. 3
2.0	16.21	28.28	33.85	47.23	38.57	39.86	38.75	34.61	14.70	(7.5 m)
1.5	16.07	25.79	27.27	38.45	32.95	30.81	32.21	31.57	13.00	
1.0	12.52	16.83	16.58	24.10	25.03	20.70	20.00	22.80	11.32	
.5	10.68	12.04	11.41	14.03	14.00	13.88	13.00	12.28	9.83	
.1	11.16	12.82	11.69	12.43	13.11	13.99	12.16	10.26	10.75	
4.0	11.42	14.93	24.51	28.66	31.57	28.89	27.59	20.22	12.51	
3.5	12.37	14.60	26.16	28.60	29.62	28.27	27.39	21.17	11.53	
3.0	12.79	14.22	23.05	28.50	29.25	27.34	28.02	21.17	10.97	Line no. 4
2.5	12.72	15.13	20.31	26.90	27.87	23.64	27.60	20.02	9.80	(10.0 m)
2.0	11.34	13.74	18.12	23.31	24.88	19.89	23.96	16.78	11.51	
1.5	9.42	12.21	14.33	16.60	20.82	16.00	19.95	13.71	9.08	
1.0	9.72	10.29	11.49	13.58	15.80	12.49	11.20	10.55	9.02	
.5	8.14	8.89	9.52	10.96	11.70	10.58	9.65	9.01	9.49	
.1	12.17	10.30	10.69	11.47	11.83	11.00	10.73	10.86	10.92	
4.0	9.45	14.32	18.92	20.68	21.15	21.01	20.28	14.03	8.31	
3.5	10.15	12.34	15.45	19.85	21.09	19.05	19.85	13.80	7.81	
3.0	11.44	12.50	14.56	18.53	21.39	17.31	19.05	13.47	7.91	Line no. 5
2.5	9.95	13.10	13.18	15.52	19.89	15.41	18.19	12.24	7.33	(12.5 m)
2.0	10.07	11.59	12.79	12.85	16.37	12.91	15.69	11.12	7.04	
1.5	8.27	8.91	10.39	9.86	12.86	11.42	12.78	11.30	7.73	
1.0	8.30	9.30	11.27	8.67	10.33	9.94	9.50	8.83	8.14	
.5	8.45	9.21	9.89	8.59	10.17	9.07	9.11	8.53	8.57	
.1	11.12	10.00	10.27	9.98	11.35	10.93	10.49	10.14	10.60	
5.0	9.65	11.14	14.17	15.50	16.99	15.70	14.28	10.56	8.86	
4.5	9.02	10.77	12.81	14.60	16.54	15.60	14.67	10.14	8.42	
4.0	9.85	11.31	13.08	14.70	15.52	15.21	14.20	10.10	8.40	Line no. 6
3.5	9.78	9.38	12.14	12.84	15.41	14.22	13.76	10.11	8.49	(15.0 m)
3.0	9.36	9.55	11.44	10.78	15.11	12.34	13.40	9.50	7.86	
2.5	9.12	8.30	8.95	10.65	13.47	10.65	12.03	7.97	7.66	
2.0	9.87	7.80	8.82	9.50	10.50	11.22	10.35	7.77	7.25	
1.5	8.64	7.26	8.38	8.58	8.59	11.63	8.99	7.64	7.57	
1.0	8.30	8.26	8.70	8.50	7.69	9.28	7.93	7.15	7.95	
.5	9.56	8.64	8.39	8.46	8.10	7.85	7.78	7.32	8.95	
.1	10.26	9.60	9.30	9.00	9.50	9.93	8.17	8.16	9.03	

Calendar Day/Time: 278/1245

No. of Burners, N = 36

Nominal Burner Power, Q = 0.130 MW

Circle Diameter, L = 4.0 m

Ambient Temperature, T_0 = 7.5°C

FIGURE 5(f): 10-Minute Temperature Means (1984)

Compass Bearing (degrees)	340	330	320	310	300	290	280	270	260	
3.0	0.00	0.00	0.00	0.00	0.00	0.00	0.00	0.00	0.00	
2.5	0.00	0.00	0.00	0.00	0.00	0.00	0.00	0.00	0.00	
Sensor Height (metres) 2.0	0.00	0.00	0.00	0.00	0.00	0.00	0.00	0.00	0.00	Line No. 1
1.5	0.00	0.00	0.00	0.00	0.00	0.00	0.00	0.00	0.00	(2.5 m)
1.0	0.00	0.00	0.00	0.00	0.00	0.00	0.00	0.00	0.00	
.5	0.00	0.00	0.00	0.00	0.00	0.00	0.00	0.00	0.00	
.1	0.00	0.00	0.00	0.00	0.00	0.00	0.00	0.00	0.00	
3.5	19.92	22.39	27.80	25.37	25.94	23.96	22.00	20.10	18.30	
3.0	20.01	24.75	27.00	27.89	31.97	28.00	22.52	22.62	20.63	
2.5	24.75	29.37	34.15	35.01	35.67	32.45	25.02	27.09	25.52	Line No. 2
2.0	26.09	33.83	37.41	36.23	35.00	37.46	27.23	27.53	21.97	(5.0 m)
1.5	21.82	29.19	38.29	39.90	40.93	40.02	27.65	25.00	20.48	
1.0	24.18	30.00	35.61	35.08	33.85	33.98	23.04	23.29	18.68	
.5	15.85	22.00	27.72	22.00	22.19	19.74	15.18	18.04	13.52	
.1	14.90	14.77	15.51	16.80	14.92	14.87	12.62	15.24	12.72	
3.5	16.66	20.13	19.91	17.73	17.73	18.00	15.98	16.85	16.15	
3.0	17.03	21.69	19.64	17.15	17.70	18.92	17.80	16.99	15.79	
2.5	15.92	21.30	21.90	18.00	17.72	19.50	18.35	16.69	16.27	Line No. 3
2.0	14.95	20.21	22.04	19.10	16.55	20.80	18.14	16.77	16.46	(7.5 m)
1.5	14.85	18.82	19.84	16.87	15.12	18.96	15.59	15.29	14.90	
1.0	13.50	16.45	15.78	13.02	13.50	16.81	13.00	13.48	13.26	
.5	12.10	13.39	11.79	12.28	13.00	12.46	12.20	11.14	11.50	
.1	12.05	12.97	11.83	12.47	12.05	12.12	11.34	11.50	11.23	
4.0	12.83	13.24	14.47	13.94	16.96	14.23	13.05	14.72	13.62	
3.5	13.57	13.91	15.68	13.70	14.33	14.81	13.44	14.60	13.19	
3.0	13.27	15.03	15.79	13.74	14.60	15.54	13.54	13.90	13.30	Line No. 4
2.5	12.65	15.81	15.13	12.98	13.90	15.26	13.55	13.35	12.76	(10.0 m)
2.0	11.99	14.54	14.25	12.87	12.70	14.27	12.81	13.33	13.06	
1.5	10.96	13.72	13.06	11.94	12.55	12.51	12.25	12.61	11.05	
1.0	11.54	11.83	11.44	11.99	11.46	11.20	11.20	11.21	10.41	
.5	9.97	10.40	10.12	11.00	10.46	10.11	9.82	10.42	10.52	
.1	12.35	11.28	10.93	11.28	11.60	11.40	11.26	11.59	12.26	
4.0	11.94	14.86	13.36	12.34	12.35	12.89	10.97	11.48	10.33	
3.5	12.29	14.11	12.00	12.10	11.58	12.49	11.54	11.50	9.95	
3.0	12.86	13.90	12.63	12.27	11.30	12.49	11.65	11.16	10.34	Line No. 5
2.5	11.50	13.89	12.57	11.52	11.31	12.11	12.06	10.80	9.80	(12.5 m)
2.0	11.58	12.79	12.19	11.09	10.58	11.20	11.60	10.95	9.35	
1.5	10.02	11.06	10.81	10.11	10.11	10.70	10.72	10.82	9.52	
1.0	10.00	10.76	11.05	9.48	9.56	10.13	10.00	9.62	9.48	
.5	9.70	10.01	10.12	9.71	10.16	9.82	9.79	10.00	9.60	
.1	11.54	10.60	10.57	10.63	11.80	11.29	11.23	11.39	11.98	
5.0	11.87	11.55	10.71	10.00	9.67	9.30	8.99	11.17	10.56	
4.5	11.55	11.37	10.69	10.30	9.83	9.80	9.88	10.71	10.16	
4.0	11.95	11.94	11.02	10.30	9.55	10.29	9.80	10.80	10.10	Line No. 6
3.5	11.51	11.02	10.89	9.42	9.65	10.34	9.73	10.86	9.99	(15.0 m)
3.0	11.38	11.18	11.12	9.21	9.69	10.03	9.94	9.50	9.61	
2.5	11.06	10.55	9.57	9.80	9.69	9.29	9.69	8.70	9.24	
2.0	10.88	10.00	9.45	9.30	9.20	9.81	9.30	8.20	9.01	
1.5	10.32	9.29	9.00	8.92	8.59	13.85	9.08	7.98	8.73	
1.0	9.45	9.57	9.45	9.00	8.18	9.35	8.72	8.08	8.80	
.5	10.25	9.39	9.32	9.25	9.00	8.53	8.82	8.53	9.44	
.1	10.55	10.09	10.00	9.87	10.10	10.61	9.56	9.69	9.89	

Calendar Day/Time : 278/1315 -

No. of Burners, N : 18

Nominal Burner Power, Q : 0.130 MW

Circle Diameter, L : 4.0 m

Ambient Temperature, T_0 : 9.0°C

FIGURE 5(g): 10-Minute Temperature Means (1984)

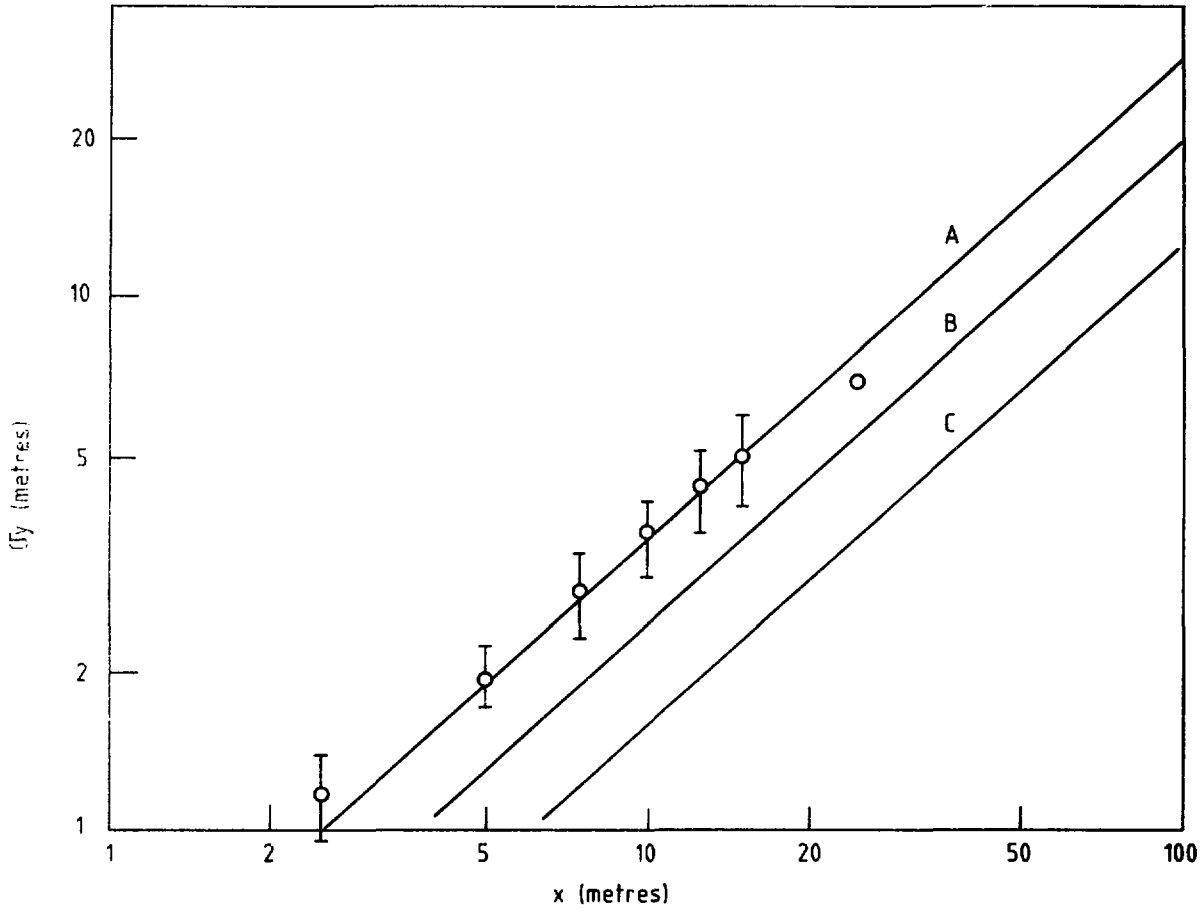

FIGURE 6: Observed Lateral Dispersion Parameter σ_y vs. Distance x Downwind from Centre of Source. Error Bars Represent $\pm$ One Standard Deviation. Pasquill-Gifford Curves for Types A, B and C Weather Superimposed (after Turner (1970))

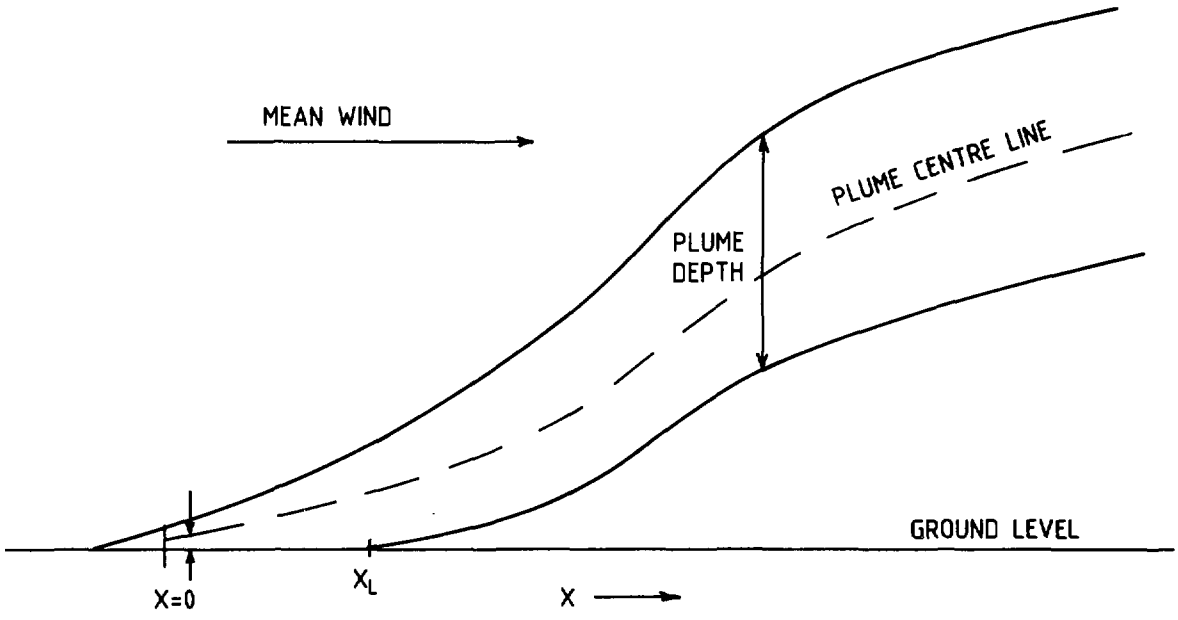

FIGURE 7: Elevation Sketch Showing General Shape of Plume. Correction for Burner Height and Jet Momentum Rise Shown At x=0

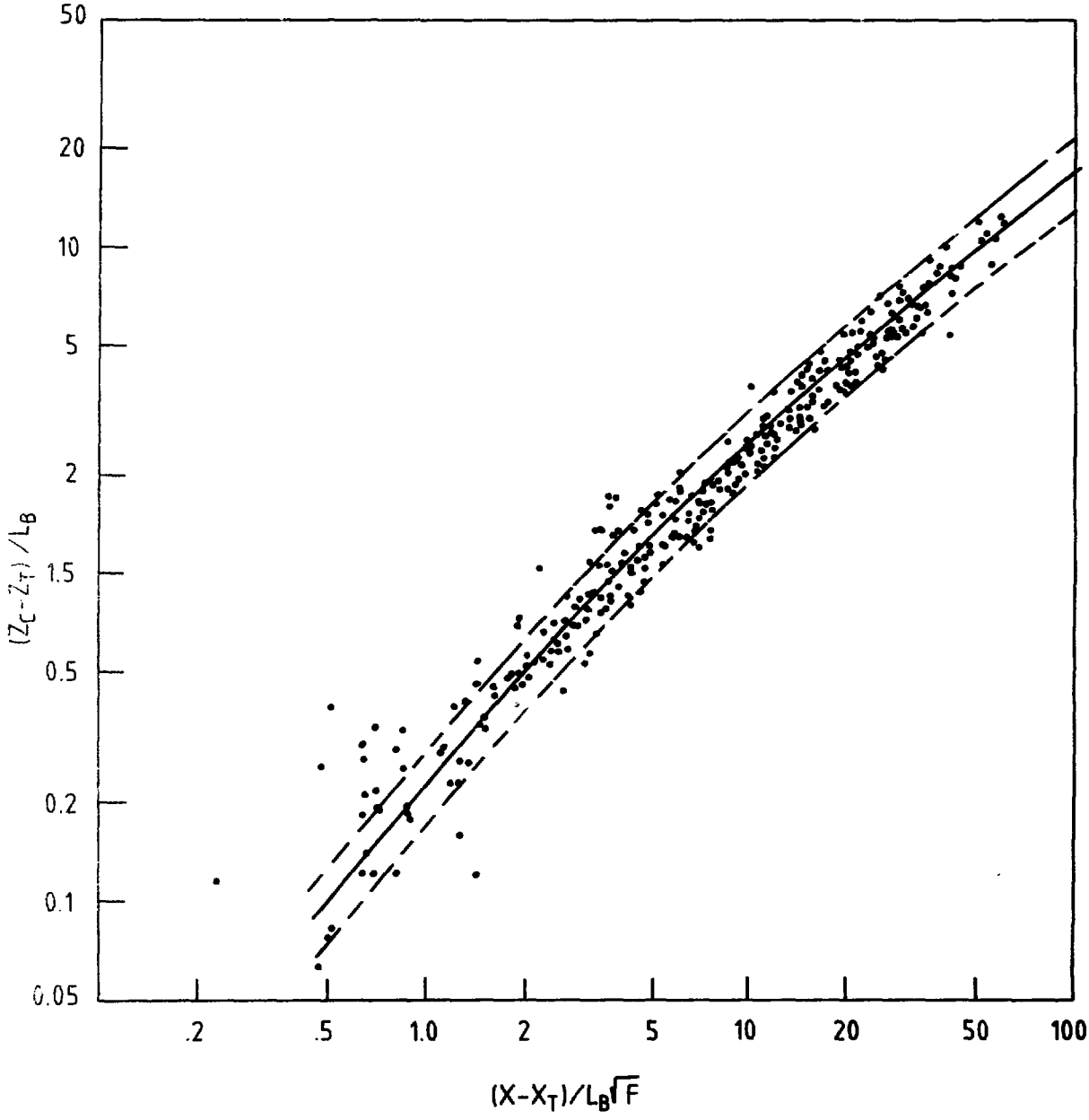

FIGURE 8: Correlations of Corrected Plume Centreline $(z_c-z_T)/L_B$ with Corrected Downwind Distance $(x-x_T)/L_B\sqrt{F}$. Middle Curve Shown with ± 25% Error Limits is given by Eq. (6.10)

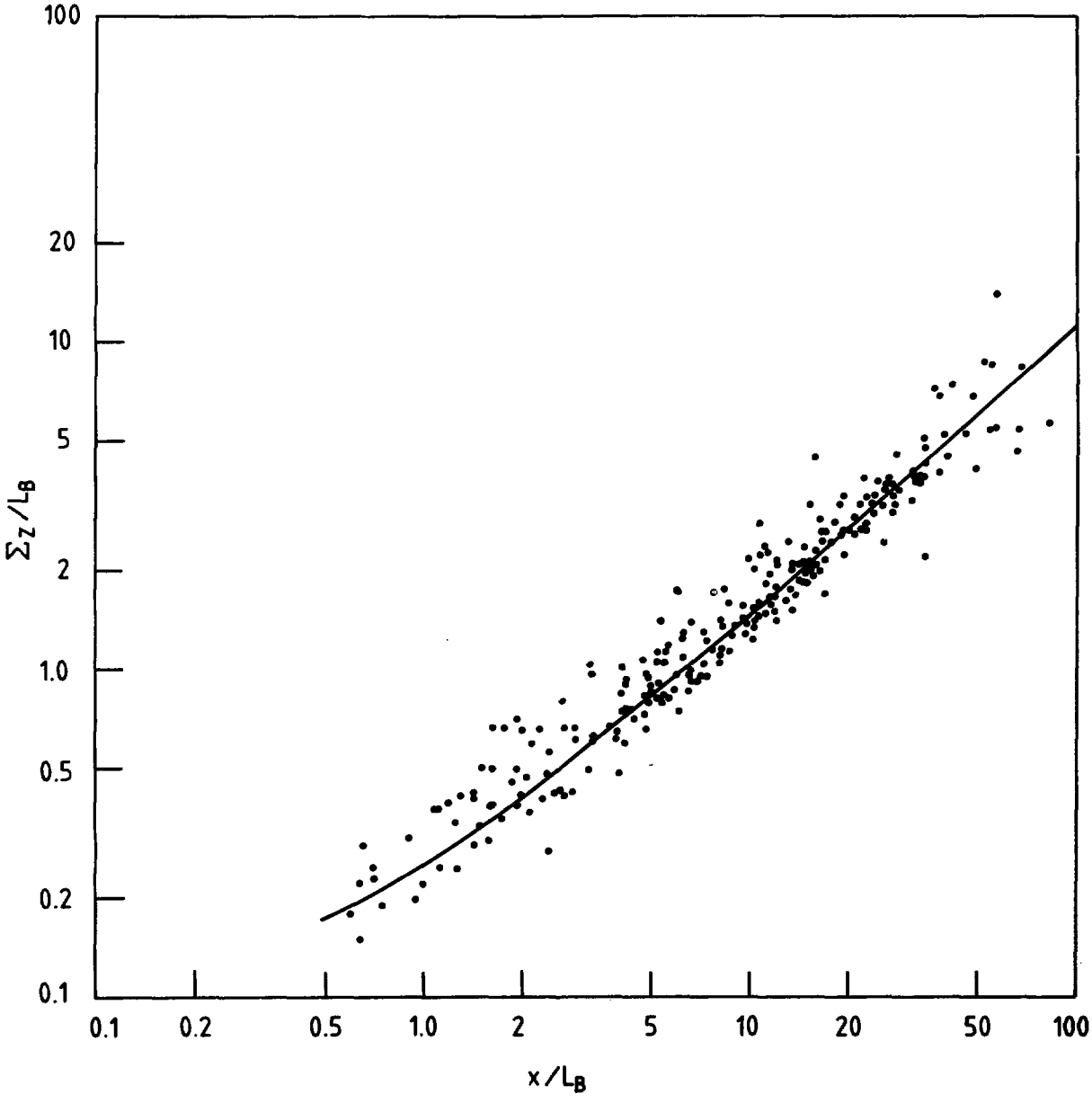

FIGURE 9: Correlation of Σ_z/L_B vs x/L_B. Curve shown is given by Eq. (7.9)

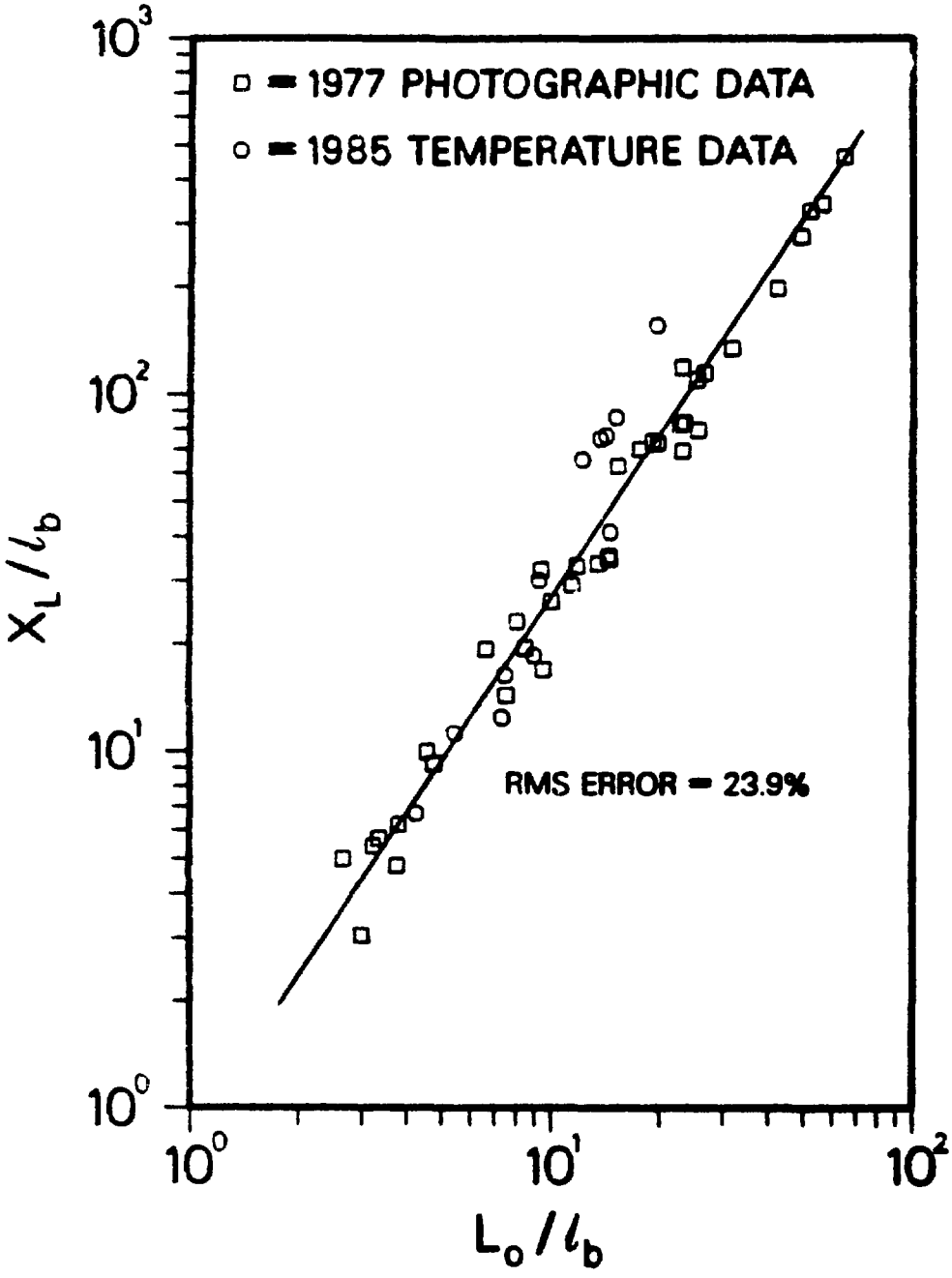

FIGURE 10: Correlation of Lift-Off Distance, Data of Slawson (1986)

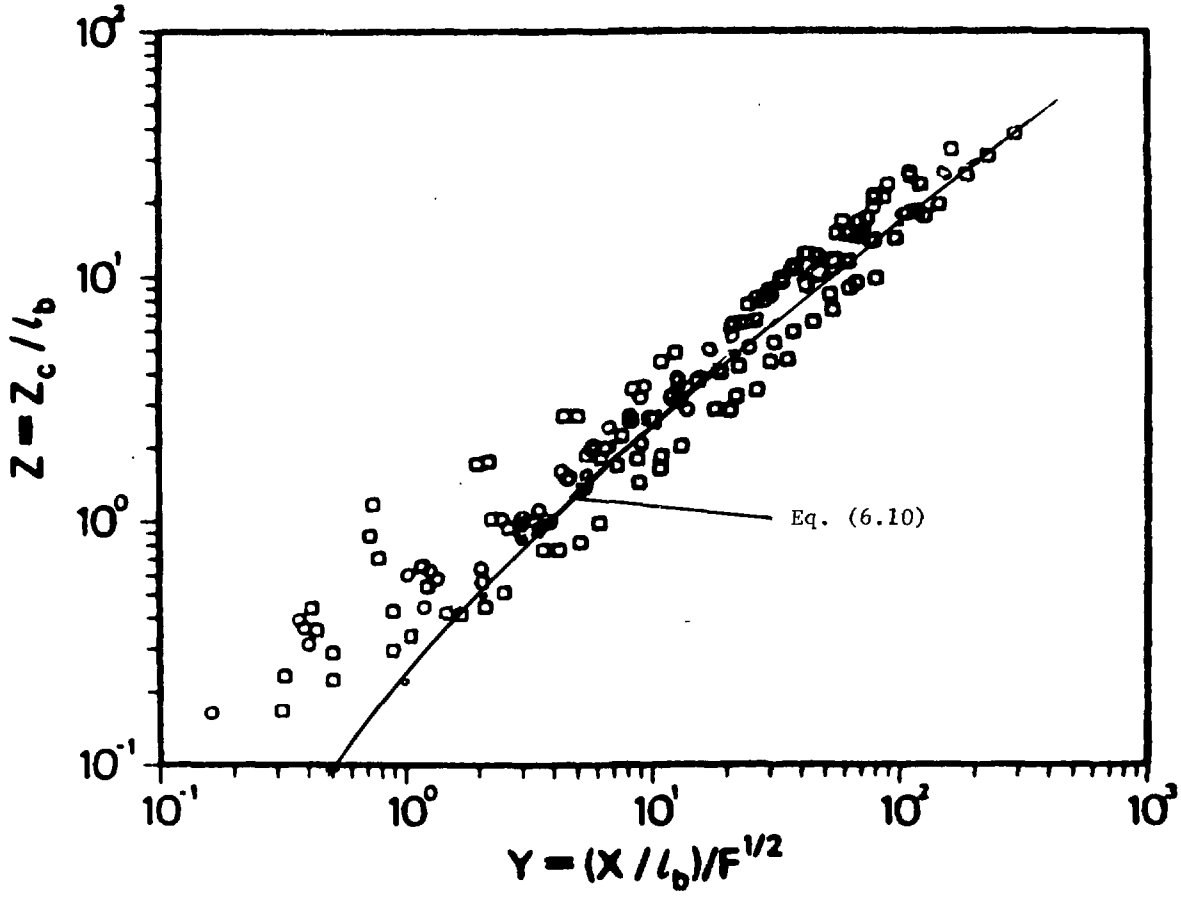

FIGURE 11: Comparison of Eq. (6.10) with data of Slawson (1986) for Centreline Trajectories from Ground Based Line Sources

APPENDIX A

PROPANE SYSTEM CHARACTERISTICS

A.1 System Description

The heat source used in the CRNL tests consisted of up to 36 propane burners supplied by Rexo-Therm Ltd. (Toronto), designed to operate at a nominal 0.15 MW (520 000 BTU/h) at 207 kPa (30 psig) header pressure. Each burner consisted of an RT-400/MS Utility Torch, including a No. 44 (0.086 in.) orifice and venturi, ending in a "T" with two burner heads that pointed upwards when the burner was laid flat on the ground. A quick-closing 1/4-turn valve and 15 ft. high-pressure hose connected the burner to the supply heater.

The propane supply system included a 3800 litre (1000 USG) bulk storage tank, 5 cm supply line, pressure regulator, isolating valves, pressure gauges and supply headers, built of Sch. 80 steel. The piping was sized to provide a reasonably low pressure drop at all flow rates, including the largest experiments with 36 burners, and to minimize the adjustments of the PRV necessary to maintain flow at a calibrated set point. The PRV was a Propane Gas Regulator, type S99-89 supplied by Fisher Controls Ltd., with cast iron body and 5 cm screwed fittings, sized to provide a flow rate up to 12 000 SCFH at a delivery pressure of 200 kPa. A parallel connection allowed a weigh tank to be used for calibration.

A.2 System Operation

It was decided to operate the system without an external vapourizer, depending on the heat capacity of the liquid propane in the tank to produce sufficient vapour for the tests. The system, therefore, required occasional recovery periods between tests, depending on the ambient temperature.

For start up, the burners were connected to the header via flexible HP hoses; care was taken to keep the hoses well away from the burner exits. The PRV was adjusted to fill the line at the desired pressure. The valve at the end of the line was then opened to fill the headers, and the propane burners were ignited one at a time by opening the 1/4-turn valve and holding a small propane torch on a boom over the burner exit. The system was shut down by closing the 1/4-turn valves one at a time or by closing the valve just before the headers. The PRV as installed generally hunted 1.0 kPa under most conditions, and became worse only when the tank pressure fell to within about 50 kPa of the set point.

A.3 Burner Calibration

The manufacturer's rating for the burners, 520 000 BTU/h at 30 psig header pressure, should be treated as nominal only. Because the flow through the orifice was choked at all pressures of interest for these tests, the mass flow rate was closely proportional to the pressure and the calibration

curve of power versus pressure was close to a straight line. Ten burners were selected at random, numbered, and calibrated in small groups of three of four, so that an average was obtained.

The burners were connected and started up as described in Section 2, and when the line pressure stabilized at the desired value, the 45 kg (100 lb) calibration weigh tank was valved in, simultaneously, closing the valve from the main tank and starting the stopwatch. At the end of the run, the weigh tank was shut off and the elapsed time noted. The runs were generally 10-15 minutes, long enough to draw a measurable amount of propane from the weigh tank and still maintain driving pressure. The tank was accurately weighed before and after the test, to the nearest 0.05 kg. It was necessary to stop some tests when the tank pressure fell too low to maintain control by PRV. The estimated accuracy of the calibration including time elapsed, weight of propane used, and pressure fluctuation, was of the order of one percent. The calibration results are given in the following table.

BURNER CALIBRATION TESTS

Test No.	Burner No.'s	Mean Header Pressure, KPa	Tank Weight Initial/Final	Elapsed Time, s	Burner Power, MW
1	1,2,3	201	78.84/ 71.30	962	0.132
2	4,5,6	201	71.30/ 62.10	1171	0.132
3	7,8,9,10	200	62.05/ 54.40	750	0.128
4	7,8,9,10	200	79.45/ 69.60	946	0.131
5	1,4,9	160	80.40/ 77.65	395	0.117
6	7,8,9,10	174	77.65/ 69.35	901	0.116
7	7,8,9,10	225	69.60/ 62.80	606	0.141
8	2,5,8	250	62.65/ 57.10	607	0.153
9	2,5,8	180	69.40/ 62.45	931	0.125
10	3,6,7,10	300	80.40/ 72.15	585	0.177
11	3,6,7,10	275	80.20/ 72.15	600	0.169

Notes

(1) The energy content of propane vapour was assumed to be 21 622 BTU/lb (50.29 MJ/kg).

(2) Header pressure fluctuated approximately ± 1.0 kPa, with exceptions as noted.

(3) Tests No. 3 and 5 were terminated when the header pressure dropped several kPa.

(4) Tank weights were determined to the nearest 0.05 kg.

(5) Elapsed times are estimated to be accurate to ± 5 seconds or less.

(6) Initial tank pressures varied from 750 kPa to 1150 kPa; final pressures from 300 kPa to 500 kPa.

(7) Ambient temperatures were in the range 23°C - 30°C during tests.

A.4 Burner Operation

Before plume behaviour near the source could be analyzed, a quantitative description of the burner flames was required. The flames from the burners are premixed and turbulent; for a general description, see [1]*, [2] and [3]. The propane vapour enters the burner as a jet from a No. 44 (0.00218 m or 0.086 inch diameter) orifice, and entrains ambient air through an aspirator. This primary fuel-air mixture then enters a venturi tube, where it expands freely without significant momentum loss, and burns after exiting through two burner ports of 0.032 m diameter. The zone of primary combustion, located immediately above the port, is ≈0.15 m long and brightly coloured. Since it is generally not possible to entrain stoichiometric air in this type of burner, the primary mixture is fuel-rich. The excess fuel not burned in the primary zone is mixed with outside air by the mechanism of jet entrainment in the secondary combustion zone, which forms a paler mantle about 0.66 m long, surrounding the primary zone. The above description was based on observations of the flames in darkness, with no wind. The observed flame length was in good agreement with predicted values [4].

A.5 Fuel Flow Through Orifice

As a check on the burner calibration, and as a means of determining the momentum of the flame, the fuel flow was calculated. The ratio of specific heats for propane vapour is $\gamma = 1.161$ ([8], p. 3-88) and the critical pressure ratio for sonic flow through an orifice is $[(\gamma + 1)/2]^{\gamma/(\gamma-1)} = 1.75$. Since the ratio of header pressure to atmospheric pressure in all the CRNL tests was well above this, the flow through the orifice was always "choked". The mass flow rate then depends only on the density ρ_h and pressure p_h of the vapour in the header and is given by

$$W_o = A_o C_D (p_h \rho_h)^{\frac{1}{2}} \gamma^{\frac{1}{2}} [2/(\gamma+1)]^{(\gamma+1)/2(\gamma-1)} \qquad \text{(A-1)}$$

where $A_o = 3.75 \times 10^{-6}$ m² is the orifice area, and $C_D = 0.82$ is a discharge coefficient which accounts mainly for the contraction of the jet in a straight-sided orifice ([9], Eq. 7.20 and Table 7.5). The propane vapour is assumed to be a perfect gas whose density is 2.02 kg/m³ at one atmosphere (101.3 kPa) and 20°C. With this assumption, the above formula predicts the mass flow rate to be proportional to header pressure and equal to 2.65×10^{-3} kg/s at a (gauge) header pressure of 200 kPa. This is in

* The numbers in square brackets are references listed at the end of this Appendix.

excellent agreement with the measured calibration curve, where the mass flow rate was found to be proportional to the (absolute) header pressure and equal to 2.60×10^{-3} kg/s at 200 kPa. The (critical) density ratio at the orifice is

$$\rho_c/\rho_h = [2/(\gamma+1)]^{1/(\gamma-1)} \qquad \text{(A-2)}$$

The volumetric flow rate at the orifice is then

$$V_o = W_o/\rho_c = A_o C_D (p_h/\rho_h)^{\frac{1}{2}} [2\gamma/(\gamma+1)]^{\frac{1}{2}} \qquad \text{(A-2)}$$

which is constant for a perfect gas and equal to $7.14 \times 10^{-4} m^3/s$.

A.6 Flow Rate and Velocity of Primary Mixture

To compute the amount of primary air entrainment, a detailed description of the flow, including momentum-pressure relations within the burner, and the pressure loss due to flame thrust, would be required. In burners of this design, flame thrust is generally small [3]. If the burner geometry does not generate large internal pressure losses, then a simple theory, which assumes no momentum loss except that occurring at the burner ports, gives the following formula ([1], ch VII)

$$V^2 = (\rho_o A/\rho A_o)\, V^2_o \qquad \text{(A-4)}$$

where V, ρ, and A are, respectively, the volumetric flow rate, density and area at the burner exit, and subscript zero refers to those quantities at the fuel orifice. As seen in the last section, V_o is constant, and ρ_o is the critical density. Since the primary entrainment is large, ρ is essentially the density of air, $\simeq 1.29$ kg/m^3 at 1 atmosphere, and since the areas are $A_o = 3.08 \times 10^{-6} m^2$ (which now includes the discharge coefficient) and $A = 1.61 \times 10^{-3} m^2$, the above formula results in a volumetric flow rate for the primary mixture that is proportional to the square root of the density (or pressure) in the header,

$$V = 0.0113 \sqrt{\rho_h} \ m^3/s \qquad \text{(A-5)}$$

At a header pressure of 200 kPa, $\rho_h = 6.01$ kg/m^3, giving $V = 0.0277$ m^3/s for the primary mixture, corresponding to a mass flow rate of 0.0357 kg/s and a burner exit velocity of 17.2 m/s. Since the mass flow rate of fuel through the orifice is 0.00260 kg/s, the primary mixture is $\simeq$7.3% by weight propane and is, therefore, fuel-rich, as expected.

A.7 Flame Trajectory in a Cross-Wind

The burners in this study were chosen for the suitability of their heat output. For buoyant plume studies, they are not ideal, since the plume originates as a jet carrying significant vertical momentum, which affects the plume rise and must be accounted for in the analysis. Fuel combustion

is a further complication. However, it has been found that the near-field behaviour of a burning jet in a cross-wind is very similar to that of a non-reacting jet [5]. In this section, a momentum correction to the observed trajectories is provided. From [6], [7] and [10], the relevant parameters, with typical numerical values, are:

D_J	jet exit diameter	(0.032 m)
U_J	jet exit velocity	(18 m/s)
U	cross-wind velocity	(2.5 m/s)
Q	burner output	(0.15 MJ/s)
g	acceleration of gravity	(9.8 m/s^2)
$\rho c_p T$	heat capacity of air	(0.38 MJ/m^3)

The following parameters are also required:

$M_1 = \pi D^2_J U^2_J/4$	momentum flux/burner	(0.26 m^4/s^2)
$B_1 = gQ/\rho c_p T$	buoyancy flux/burner	(3.9 m^4/s^3)
$L_m = M^{\frac{1}{2}}_1/U$	momentum length scale	(0.20 m)
$L_b = B_1/U^3$	buoyancy length scale	(0.25 m)
$z_1 = (M^2_1/B_1 U)^{1/3}$	mixed length scale	(0.19 m)
$z_2 = (M^3_1/B^2_1)^{\frac{1}{2}}$	mixed length scale	(0.18 m)

Bent-over jets and plumes develop in several stages, depending on the relative magnitude of L_m and L_b. If $L_m > L_b$, momentum initially dominates the centreline trajectory, which is proportional to $(L_m x)^{\frac{1}{2}}$ at first, followed by regimes characteristic of bent jet and bent plume, $(L^2_m x)^{1/3}$ and $(L_b x^2)^{1/3}$ respectively. A logarithmic plot of the centreline, therefore, follows the sequence (1/2, 1/3, 2/3) with breakpoints at $z=L_m$ and $z=z_1$. For $L_b > L_m$, buoyancy dominates at an earlier stage, so the sequence is $(L_m x)^{\frac{1}{2}}$, $(L_b x^3)^{\frac{1}{2}}$, with breakpoints at $z=L_b$ and $z=z_2$.

For the burners used in this study, it is significant that all breakpoints are close in magnitude ($\simeq$0.2 m). The middle regimes in the evolution from jet to plume will be short-lived and the plumes will tend to make the transition directly. This conveniently allows the effect of jet momentum to be removed from observed centrelines by subtraction, leaving the

remainder to be analyzed in terms of buoyancy parameters only. The initial jet trajectory is [7],

$$z_c = C_1 (L_m x)^{\frac{1}{2}}$$

where most reported observations give $C_1 = 2.1 \pm 0.3$. Therefore, the vertical correction to the observed centrelines will be $z \simeq L_m \simeq 0.2$ m, while the horizontal (downwind) correction will be $x \simeq L_m / C^2_1 \simeq 0.05$ m, which is negligible. The wind speed U for these calculations was taken at the reference height z = 0.30 m.

In a few cases, usually at low wind speeds, L_b exceeded L_m significantly (e.g., 1.0 m vs. 0.2 m) and here the appropriate correction was less obvious. Because the middle range in these cases had a 3/4 exponent not easily distinguished from 2/3, it was included as part of the buoyant regime. Thus a jet correction of L_m was applied in these cases also.

A.8 Radiation Loss from Flame

The loss of radiant energy from the primary and secondary combustion zones of the flame is small, but not insignificant. It is difficult to estimate precisely and for computing flame behaviour it is usually neglected [2]. For the present purposes, where the net amount of convective energy available to create plume buoyancy is of interest, a loss of 12% will be assumed, which is within the generally accepted range of 10%-18%; see [3].

A.9 References

[1] "Combustion, Flames and Explosions of Gases", B. Lewis and G. von Elbe, Academic Press (1961).

[2] "Flame Structure", R.M. Fristrom and A.A. Westenberg, McGraw-Hill (1965).

[3] "Flames, Their Structure, Radiation and Temperature", A.G. Gaydon and H.G. Wolfhard, Chapman and Hall (1970).

[4] "A New Criterion for the Length of a Gaseous Turbulent Diffusion Flame", T.A. Brzustowski, Combustion Science and Technology, Vol. 6, p. 313-319 (1973).

[5] "Characteristics of a Turbulent Propane Diffusion Flame in a Cross-Wind", S.R. Gollahalli, T.A. Brzustowski and H.F. Sullivan, Canadian Society of Mechanical Engineers, Transactions, Vol. 3, p. 205-214 (1975).

[6] "Turbulent Jets and Plumes", E.J. List, in Annual Review of Fluid Mechanics, Vol. 14, p. 189-212 (1982).

[7] "Mechanics of Turbulent Buoyant Jets and Plumes", E.J. List in "Turbulent Buoyant Jets and Plumes", W. Rodi (ed.), p. 1-68, Pergamon Press (1982).

[8] "Piping Handbook", M.E. Crocker and R.C. King, eds., McGraw-Hill (1967).

[9] "Applied Fluid Dynamics Handbook", R.D. Blevins and Van Nostrand (1984).

[10] "Mean Behaviour of Buoyant Jets in a Crossflow", S.J. Wright, Journal of the Hydraulics Division, Am. Soc. Civil Engineers, Vol. 103, p. 449-513 (1977).

APPENDIX B

TREATMENT OF NEAR-GAUSSIAN PROFILES

In problems of atmospheric dispersion from spatially distributed steady sources, downwind concentrations can be expressed via a superposition of sources. The usual Gaussian model then leads to error integrals and related functions. Although conceptually simple, this method is not always convenient for visualization or computation. A simple and convenient approximation is presented, based on the observation that, except in the very near field, the downwind lateral distribution is "near-Gaussian" in shape with a modified width parameter that depends on the Gaussian width σ_y and the source dimension L. The method is illustrated here for line, ring and circular area sources; it can also be applied to classical diffusion in one dimension.

B.1 Steady Horizontal Cross-wind Line Source

For a point source, the Gaussian model gives the following downwind concentration with respect to the lateral or horizontal coordinate,

$$X_o(x,y,z) = (F_o/\sigma_y)\exp[-\tfrac{1}{2}(y/\sigma_y)^2] \qquad (B.1)$$

where (x,y,z) are the downwind, lateral and vertical coordinates, F_o depends on x and z and on the wind speed, but not on y, and the source is located at the origin. A cross-wind line source, of length L with the same total output then contributes an amount dX_1' from each line element dy', that is

$$dX_1' = (F_o/L\sigma_y)\exp[-\tfrac{1}{2}(y-y')^2/\sigma_y^2]\, dy' \qquad (B.2)$$

The concentration from the entire line source is then

$$X_1 = (F_o/L\sigma_y)\int_{-L/2}^{L/2} \exp\,[-\tfrac{1}{2}(y-y')^2/\sigma_y^2]dy'$$

$$= (\pi/2)^{\frac{1}{2}}(F_o/L)\left[\operatorname{erf}\frac{L/2+y}{\sqrt{2}\sigma_y} + \operatorname{erf}\frac{L/2-y}{\sqrt{2}\sigma_y}\right] \qquad (B.3)$$

The expression (B.3) is now replaced by the modified Gaussian distribution,

$$\bar{X}_1 = (F_o/\Sigma)\exp[-\tfrac{1}{2}(y/\Sigma)^2] \qquad (B.4)$$

where Σ is a modified width parameter that accounts for the source length L; the form of (B.4) assures correct normalization. Equating (B.3) and (B.4) at y=0, and using the Taylor expansion,

$$\operatorname{erf}\eta = (2\eta/\sqrt{\pi})[1-\eta^2/3 + \eta^4/10\ldots] \qquad (B.5)$$

leads to

$$\Sigma = \sigma_y[1-(L/\sigma_y)^2/24 + (L/\sigma_y)^4/640\ldots]^{-1}$$

$$= \sigma_y[1+(L/\sigma_y)^2/24 + (L/\sigma_y)^4/5760\ldots\} \qquad (B.6)$$

The following table may be used to compare X_1 and $\bar{X}_1$, in the second-order and fourth-order approximations, for several values of the ratios (L/σ_y) and (y/σ_y).

L/σ_y	y/σ_y	LX_1/F_o	$(L\bar{X}_1/F_o)_2$	$(L\bar{X}_1/F_o)_4$
1.0	0.0	0.9598	0.9600	0.9598
	1.0	0.6059	0.6055	0.6055
	2.0	0.1519	0.1520	0.1520
	3.0	0.0150	0.0152	0.0152
2.0	0.0	1.7113	1.7143	1.7102
	1.0	1.1963	1.1873	1.1865
	2.0	0.3945	0.3944	0.3962
	2.5	0.1669	0.1726	0.1741
	3.0	0.0569	0.0628	0.0636
	3.5	0.0156	0.0190	0.0194
2.5	0.0	1.9769	1.9835	1.9729
	1.0	1.4701	1.4479	1.4450
	2.0	0.5666	0.5632	0.5678
	2.5	0.2646	0.2774	0.2818
	3.0	0.1004	0.1167	0.1197
	3.5	0.0306	0.0420	0.0435
3.0	0.0	2.1717	2.1818	2.1597
	1.0	1.7177	1.6748	1.6667
	2.0	0.7728	0.7575	0.7660
	3.0	0.1675	0.2019	0.2097
	4.0	0.0156	0.0317	0.0342

The approximation is accurate enough for atmospheric dispersion estimates provided $(L/\sigma_y)<2.5$, approximately, but deteriorates beyond there. The fourth-order terms in the expansion make no significant contribution, because where they begin to affect the result, the inclusion of even higher-order terms would be necessary; therefore, the second-order approximation is recommended for practical use. The entire approximation is best near the centre of the plume, i.e., at small values of (y/σ_y), and is less accurate in the fringes, where the Gaussian model is least reliable in any case. Although the relative error is large at the fringes, the absolute error is small there. Alternatively, the error compared to the

maximum (centre line) concentration, which is perhaps a more realistic criterion, is small. The closeness of the approximation, especially near y=0, is not unexpected when one compares the functions $\sqrt{\pi}\ \mathrm{erf}\eta$ and $2\eta/(1+\eta^2/3)$, which agree within ≃0.5% for $\eta \leq 1.6$, corresponding to $(L/\sigma_y) \leq 4.5$.

B.2 Steady Horizontal Ring Source in a Cross-Wind

For a ring source with the same output as the line source, uniformly distributed around a circle of diameter L, the simplifying assumption is made that all source elements are squeezed onto the cross-wind diameter, down-wind distance x being then referred to the centre of the ring. This is a good approximation because the dispersion parameter σ_y is nearly proportional to x in the near field, and the effects of equal displacements up- and down-wind largely cancel. With the element of line length dy' appropriately weighted to account for the circularly uniform source density, the integral expression for the concentration corresponding to (B.3) is

$$X_2 = (2F_o/\pi L\sigma_y) \int_{-L/2}^{L/2} \exp[-\tfrac{1}{2}(y-y')^2/\sigma_y^2]\ dy'/[1-(2y'/L)^2]^{\frac{1}{2}} \qquad (B.7)$$

This integral cannot be tabulated in terms of elementary functions. Assuming an expression of the form (B.4) and expanding (B.7) in powers of (L/σ_y) at y=0, gives

$$\Sigma = \sigma_y[1+(L/\sigma_y)^2/16 + (L/\sigma_y)^4/1024....] \qquad (B.8)$$

The presence of the larger coefficient on the quadratic term suggests that the approximation (B.8) is valid for smaller values of (L/σ_y), say 2.0 instead of 2.5 for the line source. The fourth-order term is again unlikely to give any significant improvement in accuracy, and the second-order approximation is recommended for practical use.

Steady Horizontal Circular Area Source in a Cross-Wind

For a circular area source of the same output and diameter L, the method leads to the second-order expression,

$$\Sigma = \sigma_y\ [1+(L/\sigma_y)^2/32] \qquad (B.9)$$

B.4 Treatment of Experimental Data

The method for analysing concentrations or temperature increments measured downwind from one of the above surfaces is to fit the observed lateral distribution to the Gaussian function, Eq. (B.4),

$$X(y) = (F_o/\Sigma)\ \exp[-\tfrac{1}{2}(y/\Sigma)^2] \qquad (B.10)$$

where Σ is the modified Gaussian width parameter for the plume. The atmospheric dispersion parameter σ_y can then be inferred from Σ by inverting the second-order approximations for the appropriate source shape and solving the resulting quadratic equation in (L/σ_y). For (B.6), (B.8) and (B.9), respectively, there results,

$$\sigma_y = \tfrac{1}{2}[\Sigma+(\Sigma^2-L^2/6)^{\frac{1}{2}}] \qquad \text{- line} \qquad \text{(B.6')}$$

$$\sigma_y = \tfrac{1}{2}[\Sigma+(\Sigma^2-L^2/4)^{\frac{1}{2}}] \qquad \text{- ring} \qquad \text{(B.8')}$$

$$\sigma_y = \tfrac{1}{2}[\Sigma+(\Sigma^2-L^2/8)^{\frac{1}{2}}] \qquad \text{- circle} \qquad \text{(B.9')}$$

B.5 Effect of Polar Grid on Measured Width Parameter

The foregoing Gaussian model is based on a Cartesian system of observations taken on lines orthogonal to the mean wind direction. A complication occurs when applying this to the CRNL field measurements made on a polar coordinate grid to accommodate, without bias, variations in mean wind direction. Over short distances, such as used here, the atmospheric dispersion parameters σ_y and σ_z are closely proportional to the downwind distance x. Thus, choosing $\theta=0$ as the mean wind direction and using the relations $x=r\cos\theta$, $y=r\sin\theta$, the horizontal temperature profiles will be of the form,

$$\Delta T = A(\sec\theta)^2 \exp[-(\tan\theta)^2/2\Sigma_\theta^2] \qquad \text{(B.11)}$$

where $\Sigma_y \simeq r\Sigma_\theta$.

If θ does not exceed about 20°, the following approximations are of acceptable accuracy,

$$\theta \simeq \sin\theta \simeq \tan\theta, \quad \cos\theta \simeq 1.0 \qquad \text{(B.12)}$$

In that case (B.11) simplifies to

$$\Delta T = A \exp[-\tfrac{1}{2}\theta^2/\Sigma_\theta^2] \qquad \text{(B.13)}$$

For example, at distances between 1 and 10 km, σ_y/x is generally 0.1 or less in neutral or slightly unstable weather, and the "plume edge", conventionally defined as 10% of the maximum is at an angle $\tan^{-1}(2.15\sigma_y/x) \leq 12°$. In routine meteorological work at these distances, therefore, the arguments y and $r\theta$ are regarded as indistinguishable, and (B.13) is used.

The CRNL gird contained deviations of up to $\pm 40°$ from the prevailing wind direction. The relatively large interval of 10° dictates that all data points be utilized in the fit of the standard deviation Σ_θ to the data. Therefore, the use of (B.13) to fit Σ_θ to the field measurements represents some compromise. Noting that the term $\sec^2\theta$ in (B.11) partly offsets the variation of $\tan^2\theta$, the error is not expected to be large. It can be roughly estimated by computing the mean coordinate x taken over the unimodal distribution $f(\theta)=1-\theta/\theta_1$,

$$x = \int_{o}^{\theta 1} x(\theta) f(\theta) d\theta / \int_{o}^{\theta 1} f(\theta) d(\theta) \qquad (B.14)$$

where $x = r\cos\theta$ and $\theta_1 = 2.15\Sigma_\theta$, representing the "plume edge". For the CRNL data, the fitted value of Σ_θ was typically in the range 0.25 to 0.45 radians. The corresponding error in x/r varies between 3 to 8%. Since Σ_y is proportional to r, the effect of using data points out to the edge of the profile is to underestimate σ_y by approximately 5%, on average. This trend was confirmed by refitting a few cases using a formula similar to (B.11).

APPENDIX C

MATHEMATICAL SYMBOLS AND FORMULAS

C.1 Mathematical Symbols

The following list includes only those symbols used in the main text. Symbols used exclusively in Appendices A and B are defined therein. SI units were used throughout.

A - coefficient in plume rise equation, eqs. (4.4) and (6.4)

C - coefficient in asymptotic plume rise formula, eq. (6.9)

c_p - specific heat of ambient air

f - denotes functional relation

F - densimetric Froude number for heat source, eq. (4.3)

g - acceleration of gravity

k - von Karman's constant ($\simeq 0.4$), eq. (3.1)

L - burner array dimension, line length or circle diameter

L_B - buoyancy length of heat source, eq. (4.5)

L_m - momentum length of burner flame, Appendix A

N - number of burners in array

Q - mean input power of a single burner

T_a - absolute temperature of ambient air

$\Delta T(x,y,z)$ mean plume temperature rise downwind from heat source

$\Delta T_o(x,z)$ mean plume temperature rise on plane y=0

$U(z)$ - mean ambient wind speed at height z

U_* - friction velocity in logarithmic wind profile, eq. (3.1)

U_c - wind speed at plume centre line

(x,y,z)- Cartesian coordinates for system, with source at origin and mean wind vector along Ox

z_o - roughness length in logarithmic wind profile, eq. (3.1)

z_c - vertical centre line coordinate of plume, or "plume rise"

z_c' - plume-rise corrected for burner height and jet momentum

Δz_J - burner plume rise due to jet momentum, eq. (4.1)

X,Z - dimensionless variables in eq. (6.10) and FIGURE 8

ϵ - fraction of burner input power appearing as convective heat, i.e., not lost by radiation

ρ - density of ambient air

θ - angular variable in polar coordinate

$\sigma_y, \sigma_z, \sigma_\theta$ ambient atmospheric dispersion coefficients in Gaussian dispersion model

$\Sigma_y, \Sigma_z, \Sigma_\theta$ modified dispersion coefficients combining atmospheric and heat source effects

C.2 Summary of Formula

The mean temperature rise $\Delta T(x,y,z)$ observed downwind from an array of N heat sources of thermal efficiency ϵ and input power Q arranged on a circle of diameter L has been modelled by the modified Gaussian formula,

$$\Delta T = \frac{[\epsilon NQ/\rho c_p]}{[2\pi U_c \Sigma_y \Sigma_z]} \exp[-\tfrac{1}{2}(y/\Sigma_y)^2]\{\exp[-\tfrac{1}{2}(z-z_c)^2/\Sigma_z^2]+\exp[-\tfrac{1}{2}(z+z_c)^2/\Sigma_z^2]\} \quad \text{(C.1)}$$

The plume centre line $z_c(x)$ is given by

$$z_c = z_c' + \Delta z_J \quad \text{(C.2)}$$

where Δz_J is the correction for burner height and jet momentum, and the buoyant component z_c' is given by

$$z_c' = 0.27x/\sqrt{F}, \text{ if } x<x_T=0.6L\sqrt{F} \quad \text{(C.3)}$$

$$z_c'=0.16L/\sqrt{F} + 0.9\, L_B X^{2/3}/[1+3.0/X^{2/3}], \quad \text{if } x>x_T \quad \text{(C.4)}$$

where

$$X = (x-x_T)/L_B\sqrt{F} \quad \text{(C.5)}$$

The modified Gaussian parameter for lateral dispersion is given by

$$\Sigma_y = \sigma_y[1+(L/\sigma_y)^2/16] \quad \text{(C.6)}$$

The modified Gaussian parameter for vertical dispersion is given by

$$\Sigma_z = [\sigma_z^{\frac{1}{2}} + (0.036\, L_B)^{\frac{1}{2}}]^2 \quad \text{(C.7)}$$

ISSN 0067-0367

To identify individual documents in the series we have assigned an AECL- number to each.

Please refer to the AECL- number when requesting additional copies of this document

from

Scientific Document Distribution Office
Atomic Energy of Canada Limited
Chalk River, Ontario, Canada
K0J 1J0

Price: B

ISSN 0067-0367

Pour identifier les rapports individuels faisant partie de cette série nous avons assigné un numéro AECL- à chacun.

Veuillez faire mention du numéro AECL- si vous demandez d'autres exemplaires de ce rapport

au

Service de Distribution des Documents Officiels
Énergie atomique du Canada limitée
Chalk River, Ontario, Canada
K0J 1J0

Prix: B

1985-90